POLITECNICO DI MILANO
Scuola di Ingegneria Industriale e dell'Informazione
Dipartimento di Chimica, Materiali e Ingegneria Chimica "Giulio Natta"
Master of Science in Materials Engineering and Nanotechnology

*Master Thesis*

# Development and Characterization of the Ionic Liquid Doped PEDOT:PSS Films for Battery Application

***Ilija BOBINAC***

Supervisor: Prof. Dr. Luca MAGAGNIN
Co-supervisor: Dr. Carlo Saverio IORIO

Academic Year 2019 – 2020

# 1. Table of Content

# 2. Acknowledgements

This research work was done at the Microgravity Research Center (MRC), a part of the Physical Chemistry department of the Free University of Brussels (French; *Université Libre de Bruxelles*).

Now that this work has come to an end, I wish to express my sincere appreciation to my supervisor, Dr Carlo Saverio Iorio, as well as the entire research group, especially Vanja Mišković, Imma Greco and Fabio Iermano. I would like to thank them for all the help and this rewarding experience altogether, it was a great honor and pleasure working with them. Special thanks go to Vincenco Gallo, who selflessly helped me during the project.

Finally, I cannot thank enough my family and friends, specially my mother, Maja; my father, Danko; my brother, Luka, and my girlfriend, Jovana. They kept me going and this work would not have been possible without their support and love.

Hvala!

# 3. List of Figures

# 4. List of Tables

# 5. Abstract

The altogether rise in new technological solutions, especially in terms of digitalization, electrical appliances, electronics, wireless technologies and similar is undeniable. Consequently, new opportunities for advanced application have arisen in a variety of branches. One example of these are medical devices, such as sensors, implants, drug delivery systems, etc. These advancements represent a result of the ever-growing need for new solutions for power supply. In this work, the possibility of using PEDOT:PSS thin and thick films as a cathode in a power storage device was explored. On top of that, it was characterized how film formulation influences its conductive ability, while an alternative application for the created battery is proposed.

The research activities were divided into 4 stages. **In the first stage** it was considered doing Scanning Electron Microscopy (SEM), Energy Dispersive X-ray Spectroscopy (EDS or EDX), Fourier-transform infrared spectroscopy (FTIR) and Four-probe resistivity characterization of the thin and thick PEDOT:PSS films with two different compositions – with and without addition of copper(II)-chloride as a source of a multivalent cation. The key component making creation of films feasible was 1-butyl-3-methylimidazolium octyl sulfate ionic liquid, which had a role of a plasticizer and conductivity enhancer. **The second step** was to design a suitable battery system and test the best performing films from the first stage as a cathode of the newly formed battery. To do that, series of discharge tests were done, from which the battery discharge time, capacity, power and energy were determined. **The third stage** was to establish the working principle of the made battery by analyzing the components after the discharge using SEM, EDS and FTIR. **Finally**, a developed sensing test was performed in order to investigate the possibility of using this device as a sensor.

Obtained results led to the conclusion that the made battery with the zinc as an anode and PEDOT:PSS film as cathode does function and that it is of Zn-air battery-type. The ionic liquid indeed appeared to be vital for the film formation and its low resistivity, but the amount of added IL or $CuCl_2$ did not significantly influence the electrical performance. On the other hand, addition of the salt created change in morphology, which proved to be disadvantageous for the given purpose. Batteries with thick films showed both higher discharge voltage and discharge time, resulting in higher power and capacity, which made them favorable for this use. Results obtained during the sensing test led to the conclusion that the created system could also have this alternative application, opening the possibility for further research.

**Key words:** PEDOT:PSS, Ionic Liquid (IL), Zn-air battery, flexible battery, sensing application.

# 6. Estratto in Lingua Italiana

L'aumento complessivo di nuove soluzioni tecnologiche, soprattutto in termini di digitalizzazione, elettrodomestici, elettronica, tecnologie wireless e così via, è innegabile. Ciò offre nuove opportunità di applicazione in molti settori diversi. Un esempio di questi sono dispositivi medici, come sensori, protesi e impianti, sistemi di rilascio di farmaci e così via. Tutto ciò ha portato alla crescente necessità di nuove soluzioni per l'alimentazione elettrica in loco. In questo lavoro, è stata esplorata la possibilità di utilizzare il PEDOT: PSS, in forma di pellicole sottili e spesse, come catodo in un accumulatore d'energia. Inoltre, è stato caratterizzato il modo in cui la formulazione del film influenza la sua capacità conduttiva e viene proposta un'applicazione alternativa per la batteria prodotta.

L'attività di ricerca è stata suddivisa in quattro fasi. Inizialmente, sono state effettuate delle prove di caratterizzazione delle pellicole di PEDOT: PSS sottili e spesse con due diverse composizioni - con e senza aggiunta di cloruro di rame (II) come fonte di un catione multivalente, attraverso tecniche d'investigazione come SEM, EDS, FTIR e la tecnica a 4 punti con sonde per la resistività. Il componente chiave che ha reso possibili i film è stato il 1-butil-3-metilimidazolio ottil solfato ionico liquido, che ha avuto il ruolo di plastificante e ha potenziato la conducibilità. Il secondo passo è stato quello di progettare un sistema di batterie adatto a testare i film con le migliori prestazioni, prodotti nel primo stadio, come catodo di una batteria di nuova concezione. Per fare ciò, sono state eseguite una serie di test di scarica, da cui sono stati determinati il tempo di scarica, la capacità, la potenza e l'energia della batteria. Il terzo è stato quello di stabilire il principio di funzionamento della batteria prodotta analizzando i componenti dopo la scarica utilizzando nuovamente le tecniche: SEM, EDS e FTIR. Infine, è stato eseguito un test per verificare la possibilità di utilizzare il dispositivo creato come sensore.

I risultati ottenuti hanno portato ad affermare che la batteria prodotta con lo zinco come anodo e PEDOT: pellicola PSS come catodo funziona e che è rientra nella classe di batterie Zn-air. Il liquido ionico si è rivelato vitale per la formazione dei film e la loro bassa resistività, ma la quantità di IL o $CuCl_2$ aggiunta non ha influenzato significativamente le prestazioni elettriche. D'altra parte, l'aggiunta del sale ha causato il cambiamento nella morfologia dei film, che ha portato uno svantaggio per l'utilizzo del PEDOT:PSS come catodo. Le batterie con film spessi hanno mostrato sia una tensione di scarica che un tempo di scarica più alti, con conseguente maggiore potenza e capacità, il che li ha resi . Attraverso I risultati ottenuti durante gli ultimi test hanno suggerito che il sistema realizzato potrebbe essere utilizzato anche come sensore, aprendo la strada a ulteriori investigazioni

**Parole chiave**: PEDOT:PSS, liquido ionico (IL), batteria Zn-air, batteria flessibile, applicazione sensoriale.

# 7. Introduction

The instantaneous rise of new technologies is continually altering the meaning of the word industry. As the rapid advancements in digitalization have set new rules for communication and industrial operation, a modified type of industry, the “industry 4.0” has been created.

The term covers cyber-physical systems (CPS), the internet of things (IoT), industrial internet of things (IIOT), cloud computing, cognitive computing, and artificial intelligence. A graphical representation of the concept is given in Figure 1.

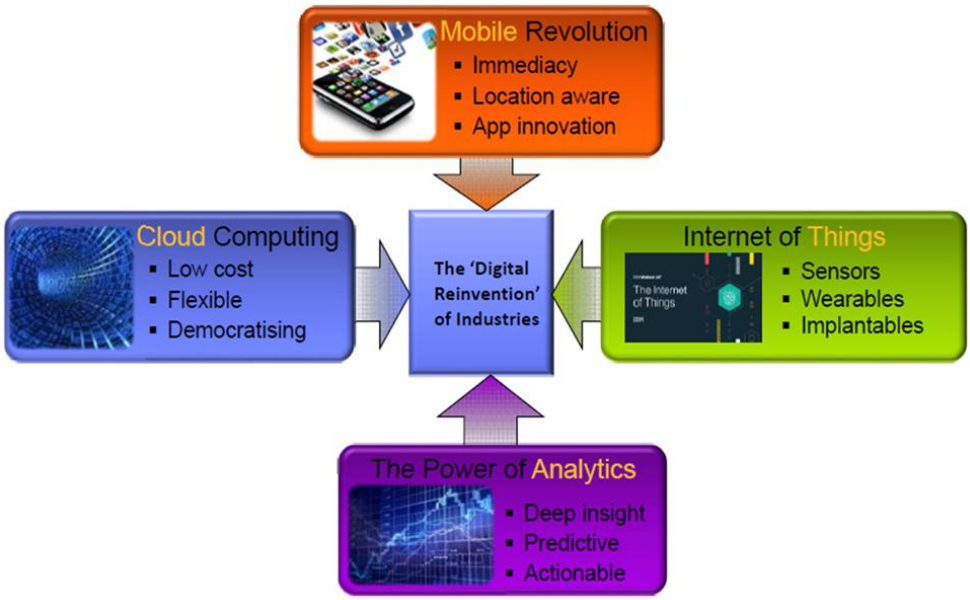


**Figure 1.** Outline of the new technologies that characterize the industry 4.0

Among all the above-mentioned branches, the internet of things (IoT) has recently attracted a lot of interest for research and development. In its main form, IoT represents the extension of Internet connectivity into physical devices and everyday objects. IoT devices open the possibility for communication and interaction with other devices via the Internet, comprising electronics, Internet connectivity, and other forms of hardware, such as sensors. Furthermore, the devices can be remotely monitored and controlled, which represents the basic principle upon which its wide application in medicine and healthcare is promising, especially in managing, monitoring and preventing chronic diseases.

The Internet of Medical Things (IoMT), thus represents the implementation of IoT systems into medical technologies, enabling practical application of the IoT in medical and healthcare environments, data collection and analysis for research, and monitoring.

The evolution of IoMT devices has significantly alleviated the complexity of monitoring systems, improved their quality and the accuracy of the results, , reduced the invasiveness of the process as well as reduced costs and improved accessibility to a large number of people.

The next level of IoMT devices will be the construction of microdevices, the miniaturized implanted medical devices (mIMDs) [1], that could potentially alter the ways in which medical emergencies are handled and significantly improve the outcomes of life-threatening situations. These devices include implantable diagnosis/monitoring capsules, microscale drug pumps, and implantable micro-sensing devices. The defining advantages of these technologies are the substantially reduced weight and size of the equipment, opening the possibility of reaching and using the micro-environments and more complex systems. The required power and working time of some of those devices are shown in Figure 2.

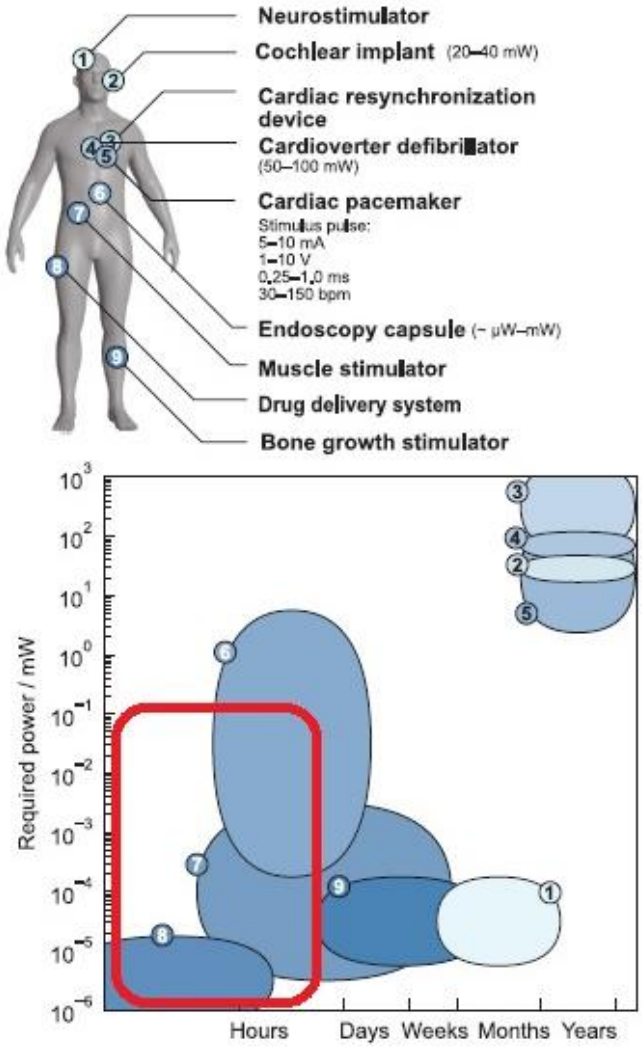


**Figure 2**. Examples of implantable medical devices and their application to different functions in the human body

To enable the efficiency and use of these new smart systems, the need for more advanced implantable power sources has become essential. Inconveniently, the shape, size and weight of

traditional implantable powers is limited, as they are produced with a layer of encapsulation in form of stiff metal shells to prevent the leakage of toxic substances. In order to make the mIMDs functionable, the key features looked for in the batteries include:

1. Micro size and weight,
2. Simple integration and implementation into the microdevices,
3. Biocompatible (Nontoxic),
4. Durable,
5. Wearable,
6. Flexible.

Figure 3 shows the principle of the new and improved implantable power source's practical application in form of smart flexible batteries.

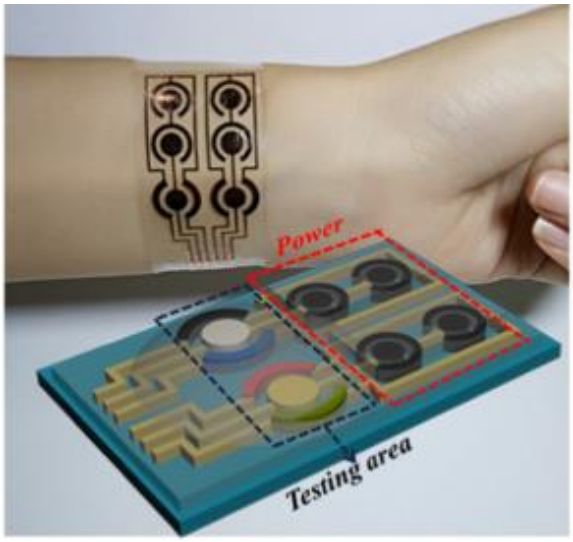


**Figure 3.** Example of a wearable sensor powered by smart flexible batteries

Considering all these required features, the need for creating a completely new type of biocompatible and implantable power source (battery) that can find its application in biomedical devices and sensors was born. Their use extends to biosensors, growth control devices, artificial organs and nerves, telemetric readings and monitoring, etc. In this manner, further development and advancement of these smart flexible batteries may completely shift the way delicate medical procedures are handled, as well as open doors for further improved of sensors and medical devices in terms of their size, weight and application.

Having said that, the main purpose of this research was to explore the possibility of using the PEDOT:PSS films with the ionic liquid as a plasticizer and conductivity enhancer for the power delivery systems and sensors, as well as to determine the effect of the film formulation on its conducting ability.

# 8. Key Features of Metal-Air Batteries

## 8.1. Introduction to Batteries

The term *battery* is very well-known and used in everyday life. Colloquially, it denotes a single galvanic cell but it could also represent an electrochemical power source (EPS). EPS is a device that produces electrical energy by directly converting energy of a chemical reaction from the process occurring in it.[2]

By using the term *galvanic* (or voltaic) cell, what is meant is Luigi Galvani and Alessandro Volta's invention. It is an electrochemical cell in which spontaneous redox reactions are occurring that as a result have charge exchange creating the electrical energy. The first cell of such kind was consisting of a copper plate and a zinc plate separated by a paper cloth soaked in salty water. These are the parts of the simplest galvanic cell - cathode, anode, electrolyte and a separator. Such system is presented in Figure 4. It is on this example that the basic working principle of the battery will be explained.

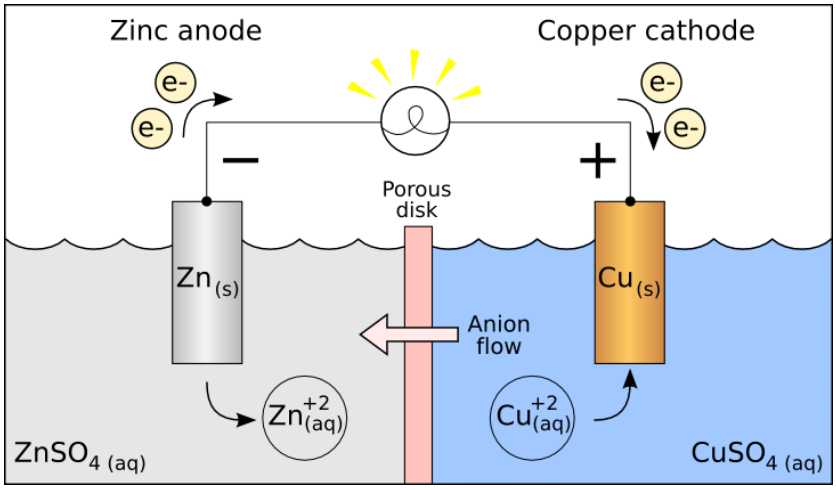


**Figure 4.** Galvanic cell with no cation flow[3]

This system can be divided into two **half-cells**. Each half-cell consists of a solid metal (electrode) that is submerged in electrolyte solution with an electrode metal cation. To complete the galvanic cell these two half-cells are connected by a semi-permeable membrane or by a salt bridge. If an external electrical conductor connects these two electrodes, the less noble metal will start to dissolve into the solution (oxidize) while releasing the electrons into the aforementioned external conductor. On the other side, the more noble metal will collect those electrons, reducing the metal ions and depositing them as metal atoms on an electrode surface. Just as it is in other chemical processes, the driving force for these electrochemical processes without applied voltage at constant T and P is a reduction in the Gibbs free energy, *G*.[4]

In this particular case, the electrochemical cell is made of a zinc (Zn) half-cell containing a solution of $ZnSO_4$ (zinc sulfate) and a copper (Cu) half-cell containing a solution of $CuSO_4$ (copper sulfate). A porous disk is used to complete the electric circuit. Following the previously described redox system, Zn (as a less noble metal) will oxidize to $Zn^{2+}$ ion and dissolve in $ZnSO_4$ solution, which makes it an anode. This will result in increased zinc ion concentration in this half-cell. In order to out this change, $Zn^{2+}$ ions will leave and $SO_4^{2-}$ anions will diffuse into the zinc half-cell through the porous disk. On the other hand, in the copper half-cell all the opposite processes will occur. On the copper electrode $Cu^{2+}$, ions from the solution will be reduced and deposited as Cu atoms on the electrode, making copper the cathode.

The two half-reactions are:

$$Zn_{(s)} \rightarrow Zn^{2+}_{(aq)} + 2e^-$$

$$Cu^{2+}_{(aq)} + 2e^- \rightarrow Cu_{(s),}$$

giving the full reaction:

$$Zn_{(s)} + Cu^{2+}_{(aq)} \rightarrow Zn^{2+}_{(aq)} + Cu_{(s)}.$$

### 8.1.1. Battery Characteristics

In order to characterize the battery, normal usage is simulated. By that, the tested cell is loaded against the known load, while the voltage difference (usually signified by ε or V) is measured. This process is called discharge and a gradual decrease of V is observed. In the Figure 5, typical voltage difference $\varepsilon_d$ vs. the time of discharge $\tau$ plots created during the discharge process are shown. These plots are called the **discharge curves.**

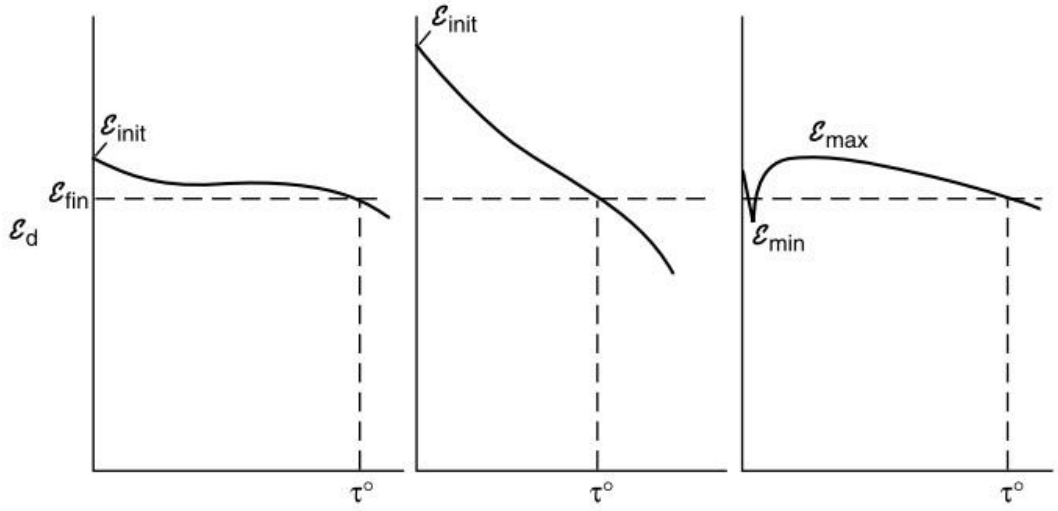


**Figure 5.** Typical discharge curves for various battery types[2]

For some of the batteries, initial decrease in voltage (up to 50%) is characteristic. This phenomenon is called the voltage falloff. It can be routed in many processes, such as higher polarization of the electrode or the increased ohmic resistance. The final voltage or voltage at discharge ($\varepsilon_{fin}$) can be reached by steep or gradual change. In order to get an accurate energy estimate, it is recommended to use the parameter of *mean discharge voltage* under given discharge conditions. It is calculated as the mean integral, or even mean arithmetic value of discharge voltage over a measured discharge time.[2], [5]

To get the **discharge power** of the battery delivered during the process, the voltage at discharge is multiplied by the discharge load:

$$P = \varepsilon_d \cdot I_d$$

Neither the discharge current nor the power output could be considered as the sole characteristics of a cell, given that both are preset by the tester.[2]

To estimate the **energy** that a battery is capable of storing, one can use the formula:

$$E = P \cdot \tau_d = \varepsilon_d \cdot I_d \cdot \tau_d.$$

Another important battery parameter is the **cell capacity**. This measure shows the total charge that can be delivered by the battery during a full discharge. It is usually given in ampere-hours (Ah).[2] If $I_d$ is load during discharge and $\tau_d$ the discharge time, cell capacity $C$ is calculated as:

$$C = I_d \cdot \tau_d.$$

In order to compensate for the difference in size, design, and electrochemical system of batteries as well as to be able to compare them, normalized (reduced) parameters are used. Such parameter is the **current density**, which serves as a measure of the relative reaction rate.[2]

### 8.1.2. Types of batteries

Based on the functioning principle, batteries are divided into:

1. *Primary batteries* –once all the reactants participating in the chemical reaction are consumed, a primary battery cannot be used any more. That is why these batteries are also called “throwaway batteries”.[2]
2. *Secondary batteries* (or rechargeable batteries) – These batteries have the ability to be recharged by applying an electric current through it, forcing the reaction to occur in the opposite direction. This process will regenerate the original reactants from the reaction

products, making it ready for another discharge. Therefore, electric energy supplied by an external power source is stored in this battery in the form of chemical energy.[2]

3. *Fuel cells* – Characteristic of these is that reactants are fed into the cell continuously while the reaction products are simultaneously removed. Having said that, the more appropriate term would be *fuel battery*, which is not commonly used. The main advantage of this device is that it can deliver a current continuously for a considerable length of time.[2]

On the other hand, batteries could also be distinguished based on the active materials in the reaction. Some of the most known are:

1. Lead-acid batteries,
2. Nickel batteries,
3. Silver batteries,
4. Lithium batteries,
5. Metal-air batteries and so on.

Since in this research the Zn-air batteries were used, which are of metal-air type, these will be discussed in more detail.

## 8.2. Basic Principles of Metal-Air Batteries

As the name suggests, these batteries utilize pure metal and air (or rather the oxygen from the air) in order to produce energy. It is an electrochemical cell where metal is an anode (so it is oxidized in this process) while an air cathode uses constantly pumped air. In this sense, it is very similar to the fuel-cell since it has an open-cell structure.

Metal air batteries first caught the attention of the researchers because of their extremely high energy density compared to the other batteries, as graphically shown in Figure 6.

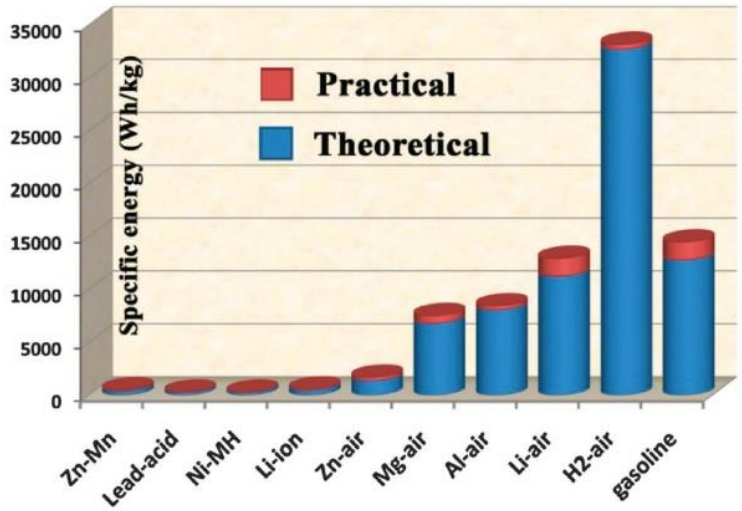


**Figure 6.** Theoretical and practical energy densities of various types of the rechargeable battery [6]

There are several ways to divide metal-air batteries: type of metal that is used, their reaction mechanism and so on, but the most common is based on the type of the used electrolyte. Therefore, there are cell systems that use aqueous electrolyte (which makes them insensitive to moisture) and the others that use electrolytes with aprotic solvents (degraded by moisture).[7]

The working principle of metal-air batteries with an aqueous medium consists of oxidizing a metal (M) into a metal oxide or a metal hydroxide, while oxygen is being reduced to hydroxide ions. The basic reactions are [8], [9]:

Positive electrode (cathode): $\frac{1}{2}\,O_2 + H_2O + 2e^- \rightarrow 2OH^-$

Negative electrode (anode): $M + n\,OH^- \rightarrow MO_{n/2} + \frac{n}{2}H_2O + ne^-$

$M + n\,OH^- \rightarrow M(OH)_n + ne^-$

Total reaction: $M + \frac{n}{4}O_2 \rightarrow MO_{n/2}$

$M + \frac{n}{4}O_2 + \frac{n}{2}H_2O \rightarrow M(OH)_n$

Similarly, in a nonaqueous medium, $M^{n+}$ species formed by oxidation go to the positive electrode to form $MO_{n/2}$ giving the same final reaction.[8] This entire process is schematically shown in Figure 7.

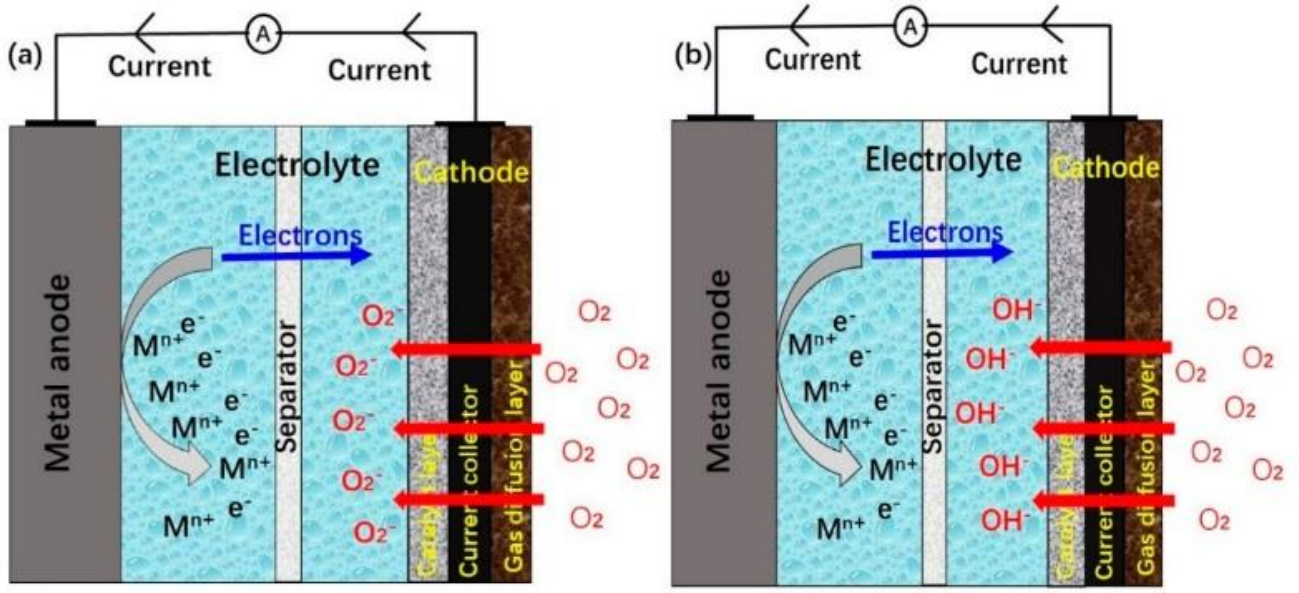


**Figure 7.** Schematic diagrams of metal-air batteries working principles for (a) non-aqueous electrolyte, and (b) aqueous electrolyte [10]

Recent progress in electric mobility caused an increase in demand of suitable energy storage solutions, especially with state of the art Li-ion batteries approaching its limits.[11] This inspired even more work towards usable metal-air batteries, leading to different solutions and different material usage.

## 8.3. Used Materials

### 8.3.1. Anode

The discharge capacity of the battery is determined by the chemical activity of the metal anode. This is the reason why choosing the right anodic material, as well as making the right combination with the other battery components, represents the key phase of the energy storage device design.

The most used materials are zinc and lithium, but aluminum and magnesium are also utilized. Given that metals generally have high activity, usage of high purity metals is suggested. On the other hand, careful combination of metals could have beneficial effect. One example would be an addition of minor spices, such as In, Pb, Cd and Hg to the Zn anode, resulting in a lower self-discharge.[12]

The biggest issues with the metal anodes are:

1. Corrosion - it is the most common side reaction. It represents the oxidation of a metal electrode, resulting in a metal-oxide or hydroxide, followed by hydrogen evolution. ;
2. Passivation - when the electrode surface is covered with an insulating layer of a metal-oxide or hydroxide, it can no longer be discharged. This process is called passivation; and
3. Dendrite formation - during discharge, the metal anode releases ions which, during the charging, get redeposited on the surface of the anode. Over time and a number of repeated cycles, the metal anode will gradually change its shape, specifically, the surface will become roughen and even the thicknesses will vary. These uneven shapes accumulate to form dendrites, resulting in an unstable battery system.[10]

### 8.3.2. Cathode

As previously stated, the reaction occurring on a cathode is a reduction of the oxygen coming from the air. Given that the oxygen reduction reaction (ORR) is a rather slow process, a catalyst for this reaction is needed. Also, when aqueous electrolyte is used, water loss should be avoided in order to secure battery stability and functionality. Taking all this into account, there are three components of the cathode (Figure 8) [10]:

1. **Gas diffusion layer** - has a range of different roles, such as supporting the catalyst layer, providing oxygen diffusion channels between air and catalyst layer, preventing water from getting into the battery, as well as the electrolyte getting out of the battery. In order to achieve maximum performance, it should be thin, light, highly porous, and hydrophobic. [10];
2. **Catalyst layer** - bifunctional catalysis is a key component of the air cathode, given that without its presence, ORR and OER are very slow. In order to increase the catalytic effect, a number

of different approaches were taken. This resulted in the usage of many different material categories, such as transition-metal compounds [13], [14], [15], double layered hydroxides [16], spinel compounds [17], [18], [19], as well as carbon-based materials [20], [21]. Generally speaking, the nano scaled ones performing better.[6], [10], [22]; and

3. **Current collector** - it should be some highly conductive material able to conduct the excess electrons form during the process.

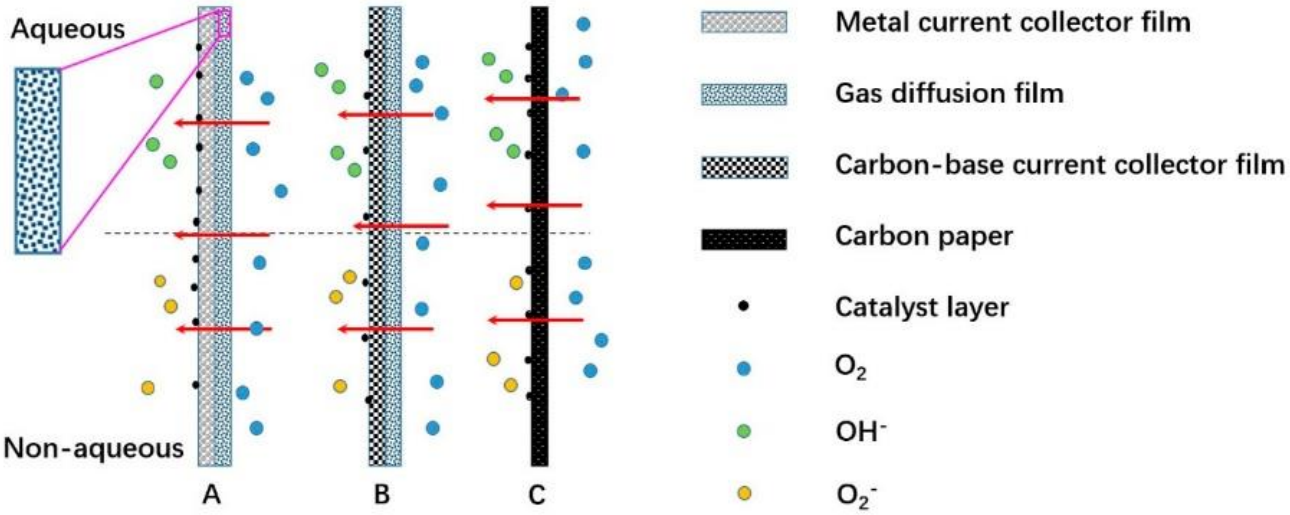


**Figure 8.** Various cathodic electrodes of MABs, (A) the metal current collector with a gas diffusion layer and the coated catalyst facing the electrolyte, (B) a carbon-base current collector and gas diffusion and catalyst, (C) a carbon paper-current collector and gas diffusion and catalyst [10]

### 8.3.3. Electrolytes

These batteries, just as all the others, have electrolytes which have the basic role of charge transport in order for the redox reaction to occur unencumbered. Typically, they are divided into two groups:

1. Aqueous electrolytes ($7 < pH \leq 14$)- as the name suggests, these are water solutions of different salts.
    a. Alkaline solution - in these solutions ORR is more favorable compared to the acidic solutions, which led to these solutions being the most applied ones. The disadvantage of using alkaline solutions is that $CO_2$ from the atmosphere forms carbonates when pH is more than 7, resulting in its deposition on the cathode which, in turn, results in the cathode efficiency decrease;
    b. Neutral salt solution (pH = 7);
    c. Acidic solution ($2 < pH < 7$) - these are rarely used since the increased amount of H+ in the solution opens the possibility of reactions with the cathodic metal, resulting in a reduced battery efficiency [23].
2. Non-aqueous electrolytes - these usually consider solid-state electrolytes, such as low molecular weight polymers (gels).[10]

Over the years, many other electrolytes have been proposed, such as ionic liquids[10], [24], biocompatible polymers[1], hybrid electrolytes[25] and many more. All of these solutions are done with the idea of achieving the highest rate of ORR either by increasing the oxygen solubility, or by oxygen diffusion. In Figure 9, schemes of some electrolytes are given.

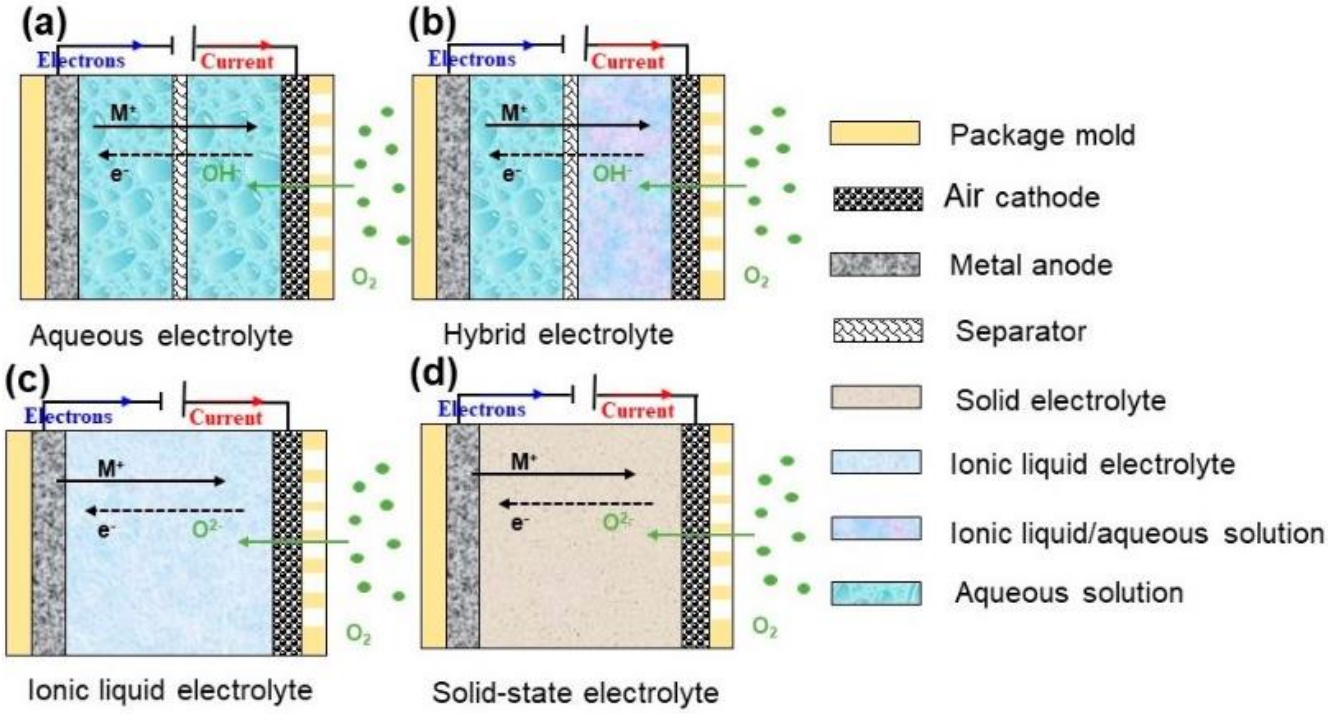


**Figure 9.** Schematic diagrams of various electrolytes of metal-air batteries[10]

## 8.4. Zn-Air Batteries

Nowadays, more than ever, we are the witnesses of an ever-increasing demand in energy. Combining that with the limited fossil-fuel resources on Earth and raising awareness of climate change, the transition to clean renewable energy is inevitable. This is why in the near future energy-storage systems will play a key role in the possibility of overall development.

Even though the Zn-air battery is essentially a century-old technology and even rechargeable systems based on it are commercially available for decades, they have only recently attracted a wider interest of researchers (Figure 10). That is because Zn–air batteries show a rather promising performance with their large theoretical energy density, low cost and fundamental safety. [22], [26], [27] Some authors went as far to say that from technological and economical point of view, zinc-air batteries represent the only viable solution for the fast-charging electric vehicles.[28]

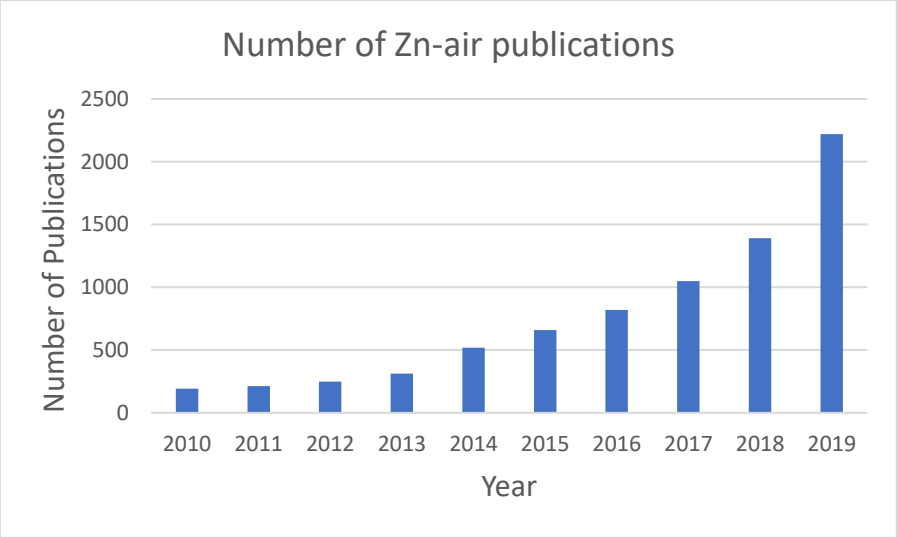


**Figure 10.** Number of publications with the topic of Zn-air batteries [29]

Although different architectures are possible, a typical one is given in Figure 11.

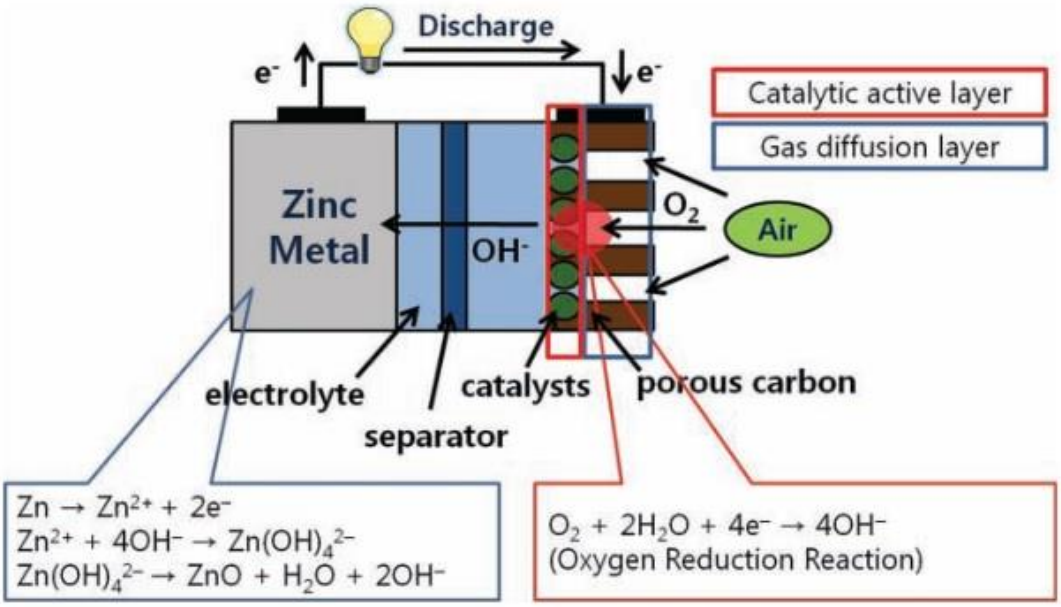


**Figure 11.** Zn-air battery architecture [7]

As represented, this galvanic-cell consists of the zinc metal as an anode, an air electrode as the cathode (divided into a gas diffusion layer and a catalytic active layer) and a separator. The red dot represents the place where the three-phase oxygen reduction reaction occurs. Due to the pressure difference between the outside and the inside of the cell, oxygen (gas phase) diffuses into the porous electrode, where it meets the catalyst (solid). Here, $O_2$ is reduced to hydroxyl ions in the alkaline electrolyte (liquid), using the excess electrons generated during the oxidation of the zinc anode. The cell reaction is completed by the hydroxyl ion migration to the zinc anode and the subsequent anode reaction. [7]

In accordance to what is presented in Figure 11 and previously for metal-air batteries, the reactions during the discharge process are [22]:

Negative electrode (anode): $Zn + 4\ OH^- \rightarrow Zn(OH)_4{}^{2-} + 2e^-$

$Zn(OH)_4{}^{2-} \rightarrow ZnO + H_2O + 2\ OH^-$

$E^0 = -1.25$ V vs. NHE

Positive electrode (cathode): $O_2 + H_2O + 4e^- \rightarrow 4\ OH^-$

$E^0 = 0.4$ V vs. NHE

Total reaction: $2\ Zn + O_2 \rightarrow 2\ ZnO$

$E_{eq} = E^0(cathode) - E^0(anode) = +1.65\ V$

Parasitic reaction: $Zn + 2\ H_2O \rightarrow Zn(OH)_2 + H_2 \uparrow$

Based on this reaction mechanism, the predicted theoretical working voltage of zinc–air battery is 1.65 V. However, as a result of the internal loss of the cell, ohmic and concentration losses, their practical working voltages on discharge are lower, typically less than 1.2 V.[22], [30]

A parasitic reaction represents a potential side reaction that can occur during the discharge. It is self-corrosion of the zinc which has a double negative effect. Not only does it lower the available active material, but it is also a potential safety hazard, given that the highly explosive hydrogen gas is produced.[22]

Zinc-air primary batteries (ZABs) have been already commercialized in hearing aids, navigation lights, and railway signals.[27] However, the secondary batteries are facing many challenges which prevent them from reaching their theoretical potential. The main goals are high-performance bifunctional catalysts, solid-state electrolytes and dendrite-free anodes which, despite the high demand for these batteries, are yet to be achieved.[22]

Since it was already discussed about the air-cathode in the metal-air segment, in this section more information about the Zn-anode will be given. Since the air for this type of a battery is supplied from the atmosphere and with that of unlimited availability, it could be said that the metallic zinc electrode is a limiting factor for the battery's capacity. A large surface area, high specific energy density, constant discharge voltage, low cost, environment friendliness and capability to withstand a high number of charge-discharge cycles are all characteristics of a prosperous electrode. [7], [22], [26]

In Figure 12, all of the disruptive phenomena that occur during the battery lifetime are schematically represented: a) dendrite growth; b) shape change; c) passivation; and d) hydrogen evolution.[26]

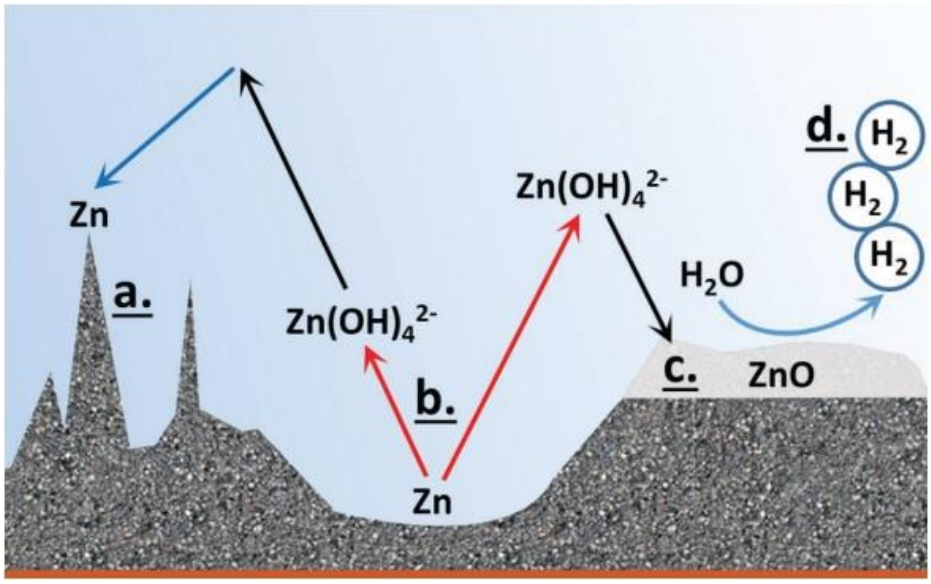


**Figure 12.** Schematic representation of performance-limiting phenomena that may occur on the zinc electrode: a) dendrite growth, b) shape change, c) passivation, and d) hydrogen evolution [26]

In order to improve performance of the zinc electrode, a number of different strategies are implemented. All the improvements are done in terms of cycle life, capacity and Coulombic efficiency (determined by the extent of hydrogen evolution).[26] These strategies are:

1. Increasing the surface area and creating a 3D electrode structure,
2. Usage of different polymer binders in order to provide mechanical stability of the powder made electrode,
3. Usage of carbon-based additives with a purpose of lowering the resistance of the zinc electrode,
4. Utilizing heavy-metal electrode additives as conductivity enhancers and current distributors in the zinc-electrode,
5. Adding discharge-trapping electrode elements, which prevent migration of the $Zn(OH)_4^{2-}$ discharge products, what in turn prevents shape change of zinc-electrode,
6. Using electrolytes with additives which could influence the surface structure of the zinc electrode,
7. Applying a coating on the electrode surface as a strategy to improve the battery life-cycle.[26]

# 9. About PEDOT:PSS

## 9.1. Introduction to Conducting Polymers

When the term *conducting polymer* is heard, one can do nothing but analyze it. First, polymers are well known, as macromolecules made of smaller units called monomers. Normally, polymers are associated with common plastics, such as polyethylene or polypropylene. Naturally, this will lead to a conclusion that conducting polymers are some of these plastics filled with some conducting additives. However, this is not the case. Conducting polymers (CPs) are structurally different molecules, which allows them to be intrinsically conducting.

The interest in CPs started with the discovery of *Shirakava et al*., that polyacetylene (PA) can achieve high conductivity for an organic molecule.[31] Although this polymer was very well known by then, but the research was not focused on the fact that it, in its regular state, expresses semiconducting behavior (conductivity~$10^{-7}$ S $m^{-1}$ compared to copper's ~$10^{8}$ S $m^{-1}$), just like all the other conjugated polymers.[32] The Shirakava and Heeger/McDiamid groups discovered that PA can develop metal-like conductivity when exposed to iodine vapors. [33], [34] This process of chemical oxidation by the halogen atom vapor, presented in the chemical reaction below, was responsible for the increase in conductivity by nine orders of magnitude up to $10^{5}$ $Sm^{-1}$.[32] This discovery led to the Nobel prize in Chemistry in year 2000, when the enormity of it was recognized.[35]

$$(CH)_n + \frac{3x}{2} I_2 \rightarrow (CH)_n^{x+} + xI_3^-$$

The process described by the above reaction is called doping. In the field of inorganic semiconductors, the term "doping" refers to the procedure of insertion of different atoms in a "pure" semiconductor in order to increase its conductivity. In the field of conducting polymers, the insertion of charges is carried out in different ways, through oxide-reduction processes, but since the resulting effect is the same (the vast increase in conductivity), the same name is also used. With that in mind, in the field of CPs, the doping can act either by extracting an electron from the valence band (p-doping) or by adding an electron to the conduction band (n-doping). Therefore, in the presented case of PA, the chemical oxidation is occurring which gives the positive species, so this is a p-doping process. [34]
The discovery of PA opened a path to a range of different conducting polymers (Figure 13). It can be seen that the variety of CPs was developed over the years, including those with different monomers, different side groups, with and without heteroatoms in the main chain, and so on.

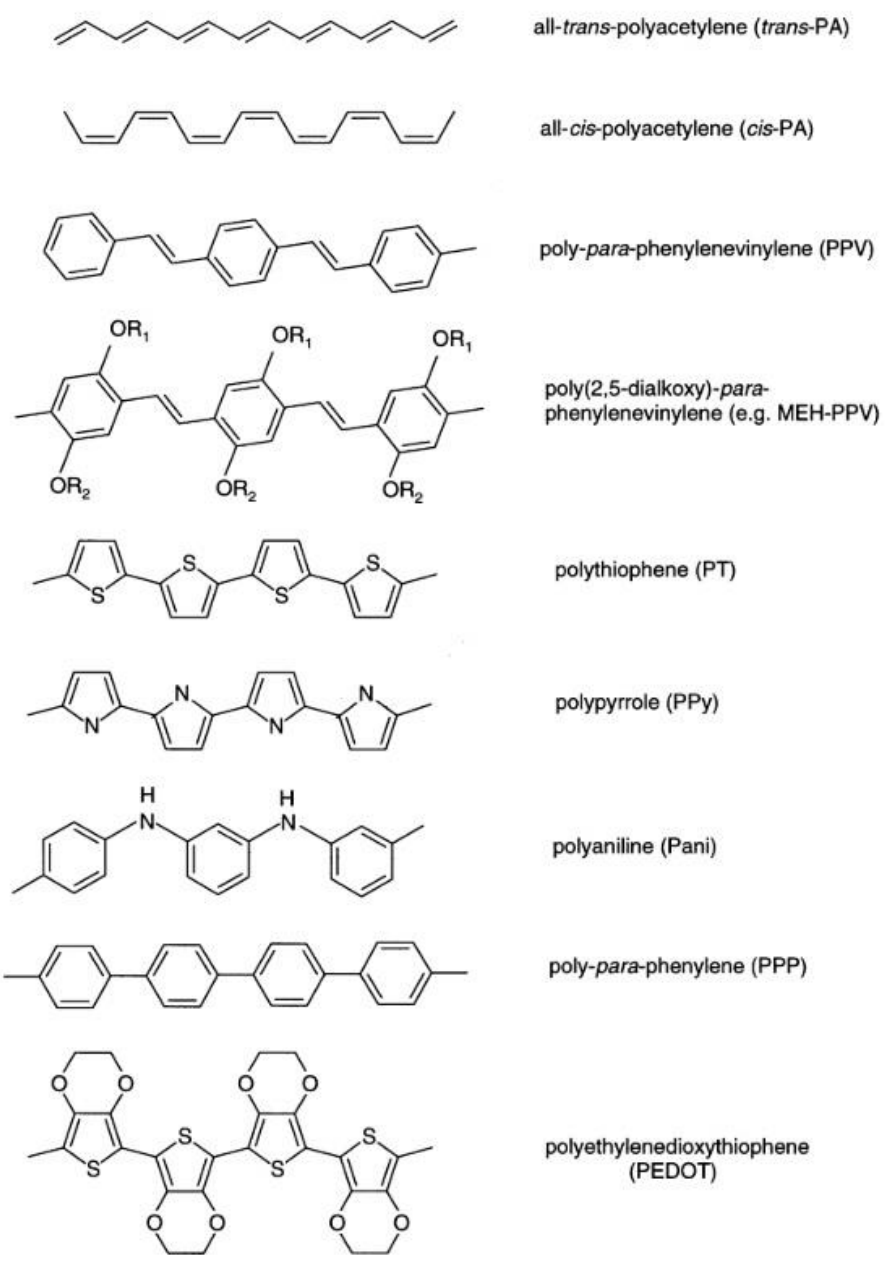


**Figure 13.** Chemical structures of some important conducting polymers [32]

Even though the variety is obvious, all these CPs share one characteristic - all of them represent conjugated polymers. These polymers are linear and planar, constituted by a series of $sp^2$ carbon atoms covalently linked to each other by alternating single and double bonds. This conjugation makes the delocalization of π-electrons along the carbon backbone possible (Figure 14). [32]

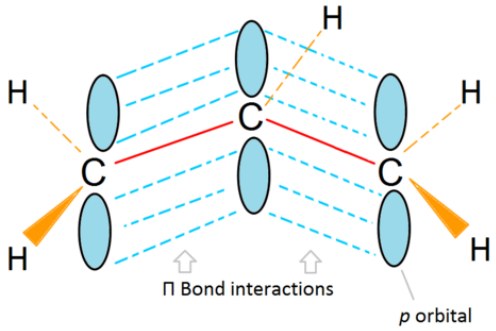


**Figure 14.** Representation of π-bond interaction in conjugated molecules [36]

The π-bands are filled and made from the highest occupied molecular orbitals (HOMO). Analogous to this, the lowest unoccupied molecular orbitals (LUMO) constitute the (empty) π*-bands. Finally, the difference between these two bands is known as the band gap energy, Eg. [32]

Even though inorganic conductors or semiconductors have superior performance and it is likely that in terms of conductivity CPs will never match them, they still have a range of desirable qualities. These include cost-effective production, lightweight, flexibility and moldability. Today, we can find CPs in many commercially available technologies, such as organic light-emitting diodes (OLEDs) for screen application, organic thin-film transistors (OTFTs) and organic solar cells (OSCs). [37] Some other possible applications with some characteristics and synthesis procedures are given in Figure 15.

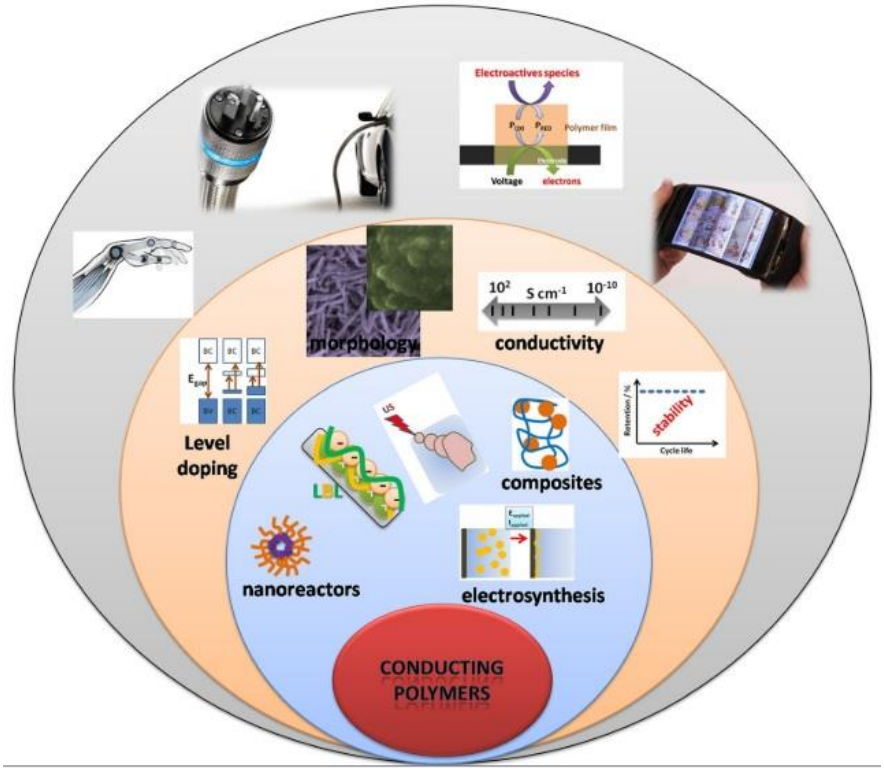


**Figure 15.** Scheme of some applications of conducting polymers with a combination of different conditions of synthesis [38]

## 9.2. Introduction to PEDOT:PSS

Poly(3,4-ethylenedioxythiophene), abbreviated PEDOT or PEDT (Figure 16) is a well-known chemically stable conducting polymer whose monomeric unit is 3,4-ethylenedioxythiophene or EDOT. The first time it was mentioned was in 1989 when Bayer applied for the patent for the preparation of polythiophenes.[37] Even though it has poor water solubility, it quickly gained researchers' interest as a most promising polythiophene in terms of conductivity, stability,

transparency and biocompatibility.[39] Nowadays, it is widely used in antistatic coatings, cathodes in capacitors, through-hole plating, OLED's, OFET's, photovoltaics, and electrochromic applications.[40]

In order to solve aforementioned solubility, different solutions are being developed. The most promising one proved to be a water-soluble poly(styrene sulfonate) (PSS). This is when PEDOT:PSS was born, a CP consisting of a positively charged, conjugated PEDOT and a negatively charged, saturated PSS (Figure 18) which had good solution-processability. It became commercially available as aqueous dispersion and developed into the most successful commercially available CP.[39]

The following paragraph explains the structure more in detail, about structure, how the structure influences its characteristics and the synthesis of the PEDOT:PSS will be said.

## 9.3. Structure and Synthesis of PEDOT:PSS

As previously mentioned, PEDOT is a part of the polythiophene group. The structure of this polymer is given in Figure 16. The mechanism underlying polythiophene's conductivity was found to be similar to that of oxidatively doped polyacetylene: generation of delocalized radicals by an oxidizing dopant, and subsequent stabilization via ionic interactions between the charged polymer and spent dopant. [37]

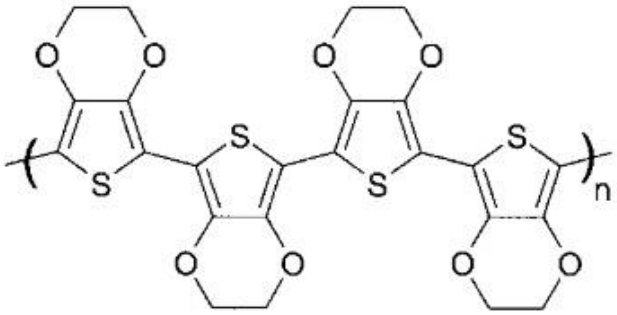


**Figure 16.** Chemical structure of PEDOT [41]

The two most important synthesis methods of PEDOT are:

1. Oxidative chemical polymerization of the 3,4-Ethylenedioxythiophene (EDOT) monomer (Figure 17) - during this process, each monomer loses two electrons and a conjugate polythiophene chain forms. There are two steps in this polymerization. First, the neutral PEDOT is synthesized via the oxidative polymerization of the monomer, followed by the second step, which is oxidative doping of the formed polymer giving the final conductive polycation. This means that under typical oxidation conditions the neutral PEDOT is not produced, but the positively charged polymer PEDOT chain. A number of oxidizing agents could be used, such as $FeCl_3$, $Fe(OTs)_3$, $Na_2S_2O_8$, and so on.[40], [41], [42];

2. Electrochemical polymerization of the EDOT monomers - this method utilizes electrochemical oxidation of the electron-rich EDOT monomer. It stands out as it requires only small amounts of the monomer and has short polymerization times, while producing finely tuned and easily controlled results. PEDOT produced by electrochemical polymerization is a highly transmissive sky-blue, doped PEDOT film at the anode. [41]


**Figure 17.** Oxidation of EDOT (Baytron M) with iron(III) tosylate (Baytron C) [40]

As previously stated, PEDOT in its neutral state is unstable, insoluble, and hard to process material. In fact, the mentioned positive charges of PEDOT obtained during polymerization need to be stabilized by counterion. In order to do so and to improve its characteristics, PSS is used. The fully stable PEDOT:PSS is produced by the oxidative chemical polymerization of EDOT in the presence of PSS using $Na_2S_2O_8$ as an oxidative agent. The resulting product is a dark blue, aqueous PEDOT/PSS dispersion, commercially available from Bayer AG under its trade name BAYTRON P (Figure 18).[41], [42]

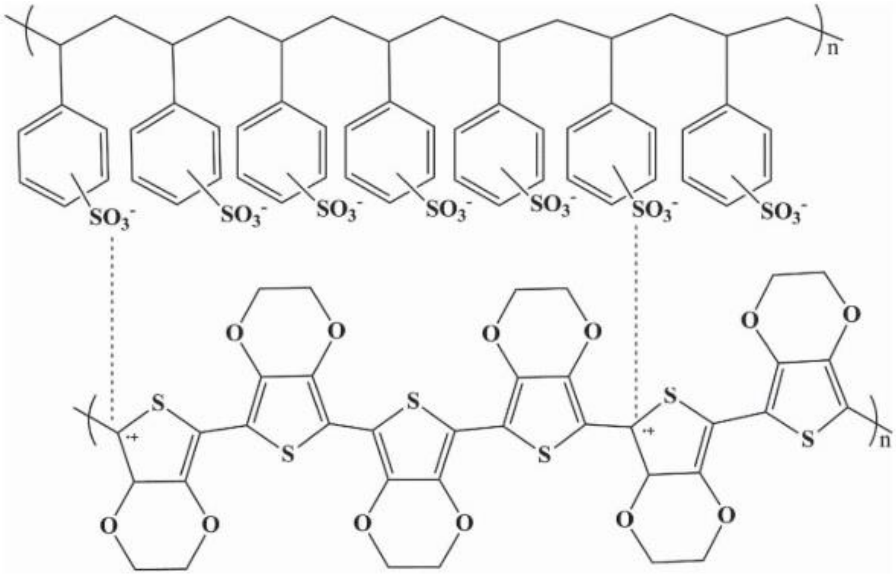


**Figure 18.** Chemical structure of PEDOT:PSS [43]

## 9.4. Secondary Doping of the PEDOT:PSS

It is a well-known fact that the film morphology and chemical and physical structure strongly influence the electrical properties of PEDOT:PSS. Because of that, a variety of post- treatments could be used in order to further improve the film performance. These methods are called secondary

doping, given that these happen after the initial doping of the material. Using some of the treatments can bring PEDOT:PSS to perform on the level of indium tin oxide, the most widely used transparent conductive material. [43] Some of the more significant results are represented in Figure 19.

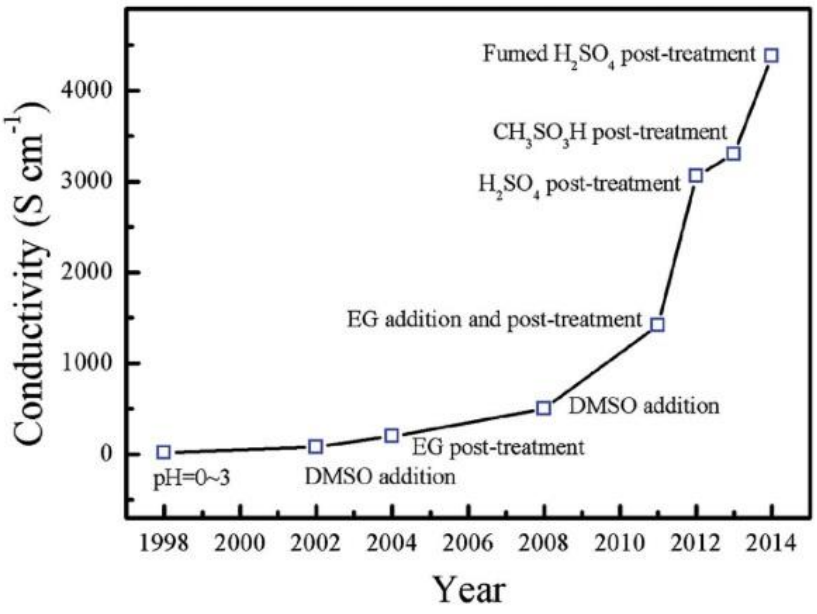


**Figure 19.** Timeline of conductivity values for PEDOT:PSS achieved by secondary doping [43]

All of the secondary doping strategies could be divided into three categories [43]:

1. Thermal treatment - different researchers reported the increase in conductivity after thermal treatments at temperatures ranging from 100 °C to 250 °C;
2. Light treatment - using the UV irradiation an enhancement in conductivity and the work function of PEDOT:PSS could be achieved. It is believed that UV irradiation causes changes in the coil conformation, as well as decrease in the number of the charge trapping related defects, which in turn leads to conductivity enhancement;
3. Chemical treatment - there are many different chemicals that are used, such as organic solvents, ionic liquids, surfactants, salts, zwitterions, and acids. The shared characteristic is that all of these are done by simple solution mixing.

It should be noted that despite all the achieved progress so far, the subject of mechanism of secondary doping is still debatable. Since in this work the ionic liquid post-treatment method was used, more about its procedure and proposed mechanism will be given in the next paragraph.

### 9.4.1. Ionic Liquids

Ionic liquids (ILs) are organic cation/inorganic anion salts with a primary defining characteristic of melting temperatures below 100 °C. Furthermore, unique properties such as good chemical stability, low flammability, and negligible vapor pressure make them widely applicable in many technological

fields.[44] Döbbelin et al. were first to report who reported the use of ILs as an additive to increase the PEDOT:PSS conductivity.[45] The treatment consists of simple mixing of water solutions and short thermal treatment on low temperatures. Presented results and simplicity of the method, combined with the environmental non-toxicity, made this procedure rather attractive for further development.[43]

The research group of professor Wang *et al.* from Stanford University was able to give the explanation of the effect of ionic liquid (here marked as STEC) on the PEDOT:PSS films.[46] Figure 20 provides a graphical representation of the obtained result.

As a result of the charge screening effect of the IL, more crystalline and more interconnected PEDOT nanofibrillar structures are formed. This is the main reason behind the increase in conductivity. Furthermore, the increase in elasticity is observed. It is suspected that IL molecules are mostly present in the more disordered regions due to the increased PEDOT crystallinity, which gives rise to a nanofiber network embedded in a soft matrix. This structure is responsible for the high elasticity and softening of the material.[46]

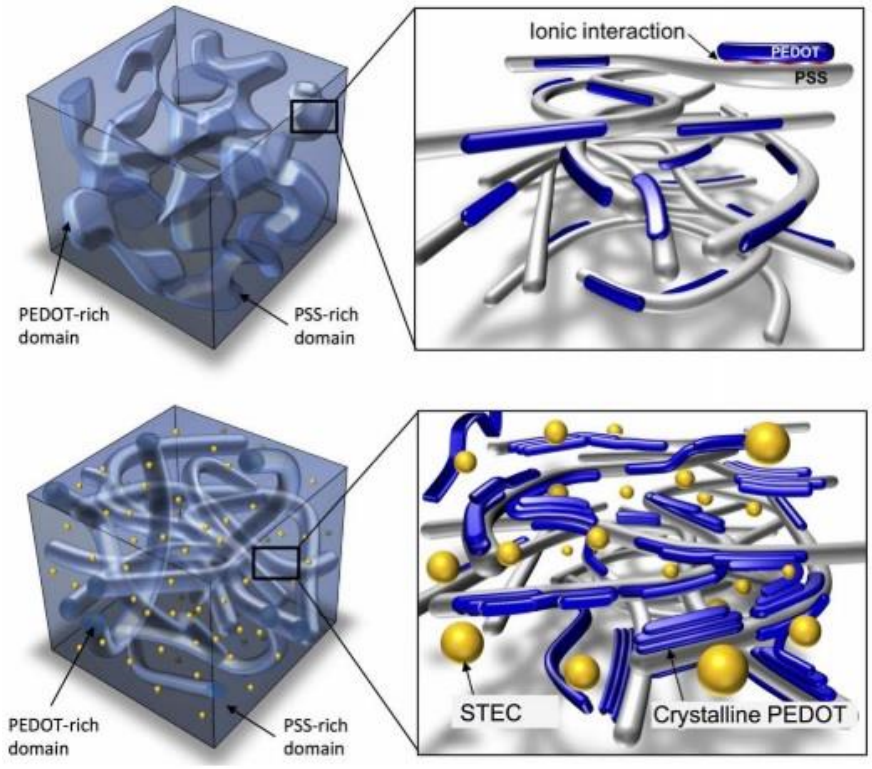


**Figure 20.** Schematic diagram representing the morphology of a typical PEDOT:PSS film (up) versus that of a stretchable PEDOT film with STEC enhancers (down) [46]

# 10. Experimental Part

In order to present this work in a structured way, the research could be divided into 4 stages.

1. Electrode Formation and Characterization

The focus of this stage was to fabricate, characterize, compare and in the end choose the optimal PEDOT:PSS form and composition in terms of electrical and mechanical performance.

A set of preliminary tests was done with the purpose of finding the optimal fabrication processes for the electrodes. After achieving that, two film forms were compared:

a. Thin films – produced on the PDMS supports,
b. Thick films – produced in Teflon molds,

as well as two films compositions:

a. PEDOT:PSS with the addition of different amounts of ionic liquid (15% to 60%),
b. PEDOT:PSS with the addition of ionic liquid and different amounts of copper(II)-chloride (1mol% to 10mol%).

2. Battery Assembly and Characterization

Since the battery is a relatively complex system, different tests were done on different designs, after which the right assembly was chosen. The influencing factor was not only the performance of the specific components but also availability and convenience.

Discharge tests were done to evaluate the performance of the battery.

3. Battery Reaction

In order to analyze the reaction which is responsible for the charge generation, post-discharge tests were done. Scanning Electron Microscope (SEM) and FTIR analyses were done on Zn-electrode, PEDOT:PSS electrode and the separator before and after the discharge, opening the possibility to compare them and get a better insight into what is the working mechanism of this battery.

4. Battery Application as a Sensor

What was noticed during the research was that the proposed assembly can have rather interesting application. Here is presented and analyzed the behavior of this assembly as a sensor for body fluids.

The scheme of the complete experimental part is given in Figure 21.

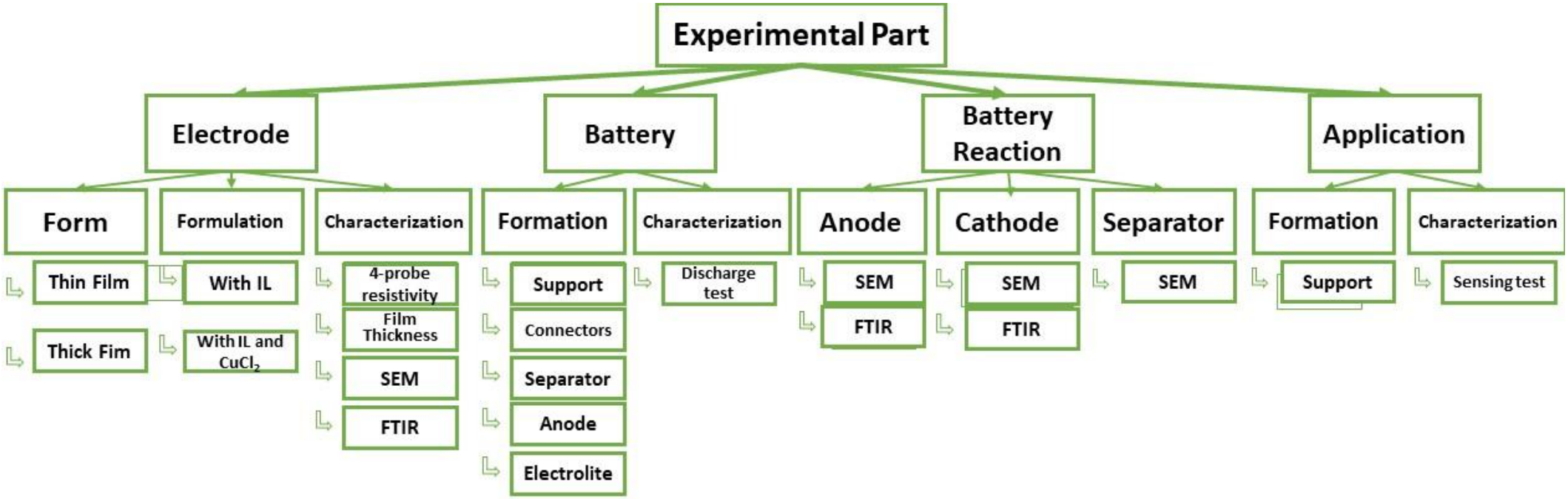


**Figure 21.** Scheme of the Experimental work

# 11. Materials and Methods

## 11.1. Film Formation

In this work, two types of PEDOT:PSS films were formed (thin and thick films) with two different compositions (with and without copper(II) chloride). The purpose of this was to find both the optimal form and formulation for the use in batteries. In next paragraphs, procedures for this were described.

### 11.1.1. Thin Films

Thin films are formed by simple mixing of components and pouring onto the PDMS supports, then drying and finally annealing. This was done in accordance with the process proposed by Wang *et al.* [46] Before using the PEDOT:PSS aqueous dispersion (*CLEVIOS™ PH 1000*), it must be sonicated for 15 minutes.

There were two thin film formulations. **The first** one was without $CuCl_2$, so it consisted of PEDOT:PSS dispersion and 1-butyl-3-methylimidazolium octyl sulfate ionic liquid (*Sigma Aldrich, ≥96% HPLC*) as both a plasticizing agent and a conductivity enhancer. The amount of ionic liquid (IL) was varied (15 w%, 30 w%, 45 w% and 60 w%) in order to determine the optimal composition. In the **second** formulation, IL addition was fixed at 45 w%, but the addition of anhydrous copper(II) chloride (*Alfa Aesar, min 98%*) differed from 1 mol% to 10 mol%, precisely 1 mol%, 3 mol%, 5 mol% and 10 mol%. After the addition of all components, mixtures were steered vigorously on a magnetic steerer for 10 minutes, after which 1 g of them was poured on each rectangular PDMS (*DOW SYLGARD 184 Silicone Elastomer Kit*) support of 10 mm width and 50 mm length.

Drying lasted for 4 hours at ambient conditions. Annealing was done in the oven at 130 $^{o}$C for 20 minutes, with gradual increase of temperature from 20 $^{o}$C to 130 $^{o}$C. The film that is formed is dark, compact, thin, attached to the support, but can easily be separated from it without breaking.

### 11.1.2. Thick Film

The thick film formation mimics perfectly the process described for thin films with the difference in the usage of Teflon molds instead of supports. Once again, it is the process proposed by Wang *et al.* [46]

After mixing, 5 g of each mixture was poured into 50 mm square and 5 mm deep Teflon molds. Drying lasted for 18 hours at ambient conditions. Annealing was done in a pre-heated oven at 130 $^{o}$C for 25 minutes. The films that were formed were dark, compact, significantly reduced in size and could easily be separated from the mold.

## 11.2. Battery Assembly

To create a battery with all its parts, which would be functional, reliable, measurable and with good performance, it was necessary to select, apart from electrodes, also the support, connectors, the separator and the electrolyte.

After careful consideration and a series of tests, the final assembly was chosen. The schematic representation of it is shown in Figure 22.

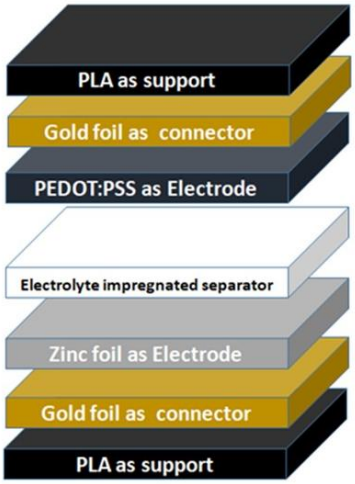


**Figure 22**. Battery components

Although the final goal of this project is in the domain of flexible electronics, for this stage of research rigid PLA was chosen to be used to fabricate supports. This was done for a number of reasons, such as ease of fabrication, versatility of possible designs, availability and possibility to provide a good contact, which is essential for battery testing.

The **PLA support** (shown in Figure 23) was modeled in the *SolidWorks 2017* software and fabricated using *Prusa i3 MK3* 3D printer. It was designed with 0.4 mm grooves to ensure good adhesion of components, as well as with air-flow channels (necessary to provide air in this Metal-air battery) and connection terminals.

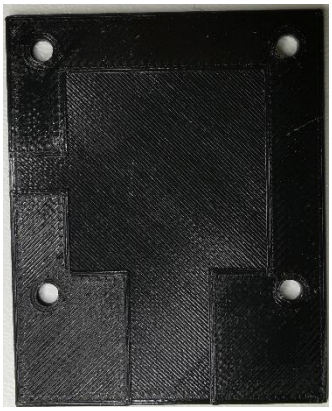

**Figure 23.** PLA battery support

To ensure good **connection** *80 µm thick gold foil* was glued directly to the PLA supports.

As the **separator** *Whatman Grade 41* filter paper was used. It was chosen for its flexibility, biodegradability, and precise pore size (20 to 25 µm). To fully prepare it for use in the battery, it was cut into 25 mm squares and immersed for 10 minutes in a phosphate buffer saline (PBS) making. A *Sigma-Aldrich sterile and filtered PBS with pH 7.4* was used for this instance as an **electrolyte**. It was suitable since it can perfectly mimic bodily fluids (e.g. blood), which was important for the battery application as the sensor.

To complete the battery, 25 mm squares of 0.25 mm thick *zinc foil*, purchased from Sigma-Aldrich was used as the **anode**. It was chosen because of its flexibility and very low surface resistance of 5.8 µΩ-cm at room temperature.

Finally, to form the battery, all these components were stacked together and then everything was secured with Teflon screws, as it is shown in Figure 24.

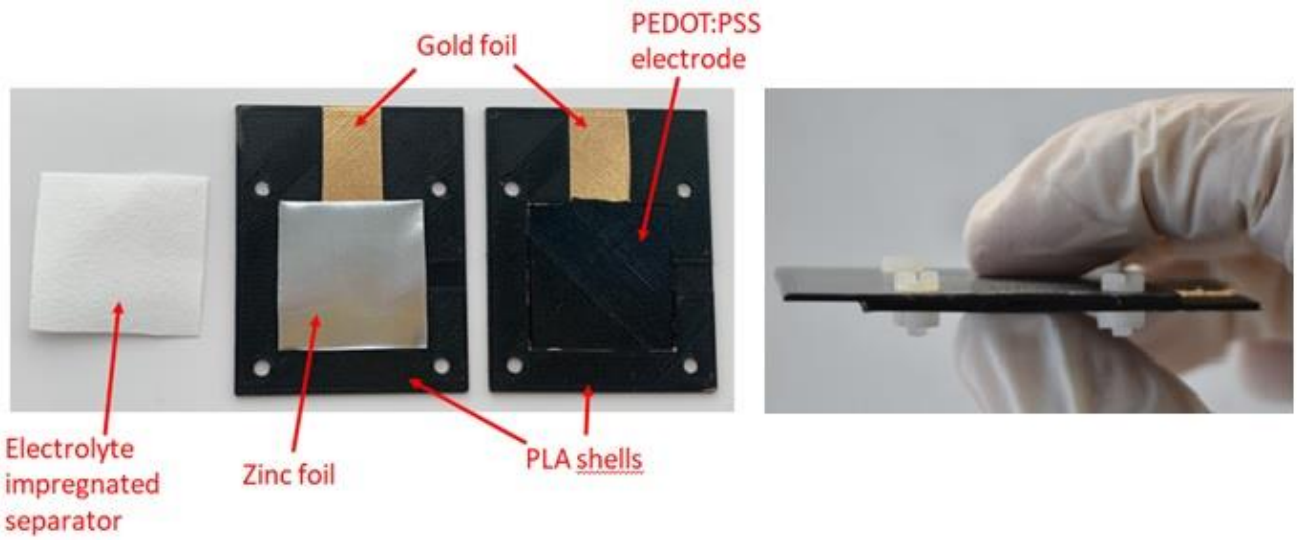


**Figure 24.** Battery assembly

## 11.3. Characterization Techniques

### 11.3.1. FTIR

The best way to describe Fourier-Transform Infrared Spectroscopy (FTIR) would be to start from its name. Fourier-Transform (FT) refers to the mathematical process utilized to convert the raw data into the usable spectrum. On the other hand, Infrared (IR) radiation is the part of the electromagnetic spectrum wavelengths (λ) from 780 nm to 1000 µm. It is usually distinguished among three subregions: near-IR region, mid-IR region, and far-IR region.

At temperatures above absolute zero, all the atoms in molecules are in continuous vibration with respect to each other. These vibrations are periodic motions of the atoms of a molecule relative to each other, without altering the center of mass of the molecule. Different ways of vibrations could be distinguished called *vibrational modes.*[47]

Furthermore, it can be said that Fourier-Transform Infrared Spectroscopy (FTIR) is a technique which belongs to the group of methods called *vibrational spectroscopies*. Since infrared radiation has the energy equivalent to the vibration of the chemical bonds, FTIR is able to exploit this fact and use it to determine the composition of materials, as well as their interconnections. This is possible by exciting the molecules in their ground state and measuring their response in one of the three modes: transmittance, reflectance, or absorbance.[48] For the vibrational mode to be observed, changes must occur in the permanent dipole. In fact, the larger the dipole change, the stronger the intensity (I) of the band in a recorded IR spectrum.[47]

For this thesis *Jasco FT/IR-6600* in ATR mode was used, so the working principle of this particular mode will be described. A scheme of such an instrument is given in Figure 25.

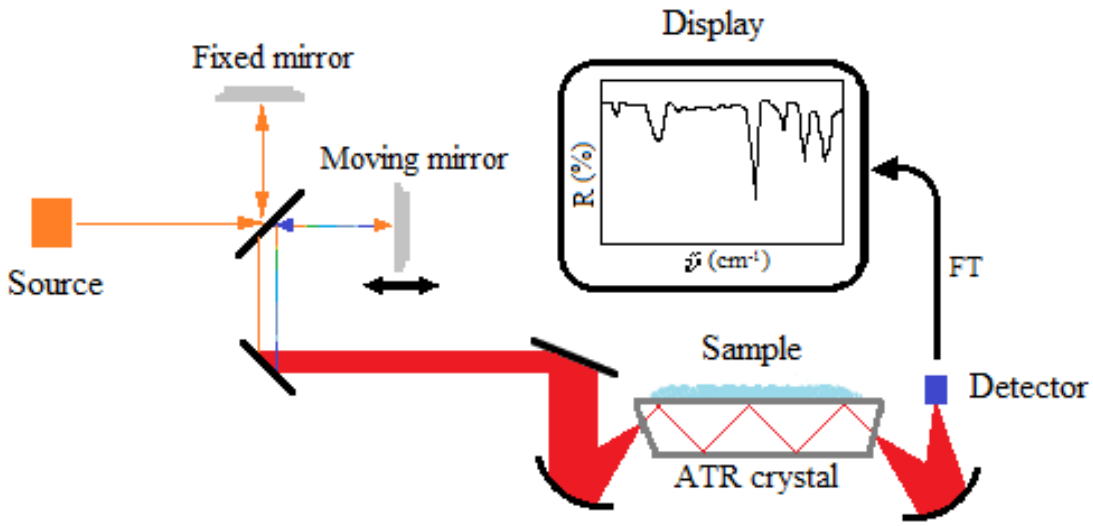


**Figure 25.** Working principle of ATR FTIR spectrometer [49]

System consisting of a source, a splitter, a fixed and a moving mirror is used to form infrared radiation with the precisely differentiated wavelengths. After achieving that, the infrared beam is directed into the Attenuated Total Reflection (ATR) crystal with another system of mirrors. The beam can propagate down the length of the crystal due to the total reflection at the surface before finally reaching the detector, as shown in the Figure 25. By doing so, the beam interacts with the sample at several points and with that, the effective path length is increased.[48]

Finally, the resulting spectra is presented as the dependence of transmittance T (%) of the wavenumber. Wavenumbers are the reciprocal values of wavelengths and are usually represented in $cm^{-1}$. The peak position is most commonly exploited for qualitative identification because each chemical functional group displays peaks at a unique set of characteristic frequencies. Comparing peak positions with one of the well-established databases will give the fingerprint that can be used to identify chemical groups and with that, complete compounds.[48]

### 11.3.2. SEM

Just like the optical microscope, a Scanning Electron Microscope (SEM) is used for detailed analysis of a material surface. A crucial difference is the use of an electron beam as a source instead of the visible light. Given that wavelength λ of the probing radiation is determining the resolution of the microscope (the shorter the wavelength, the smaller the feature that can be detected), this is making SEM a far more superior instrument, since electrons have the wavelength as short as $10^{-12}$ m compared to $\lambda = 10^{-7}$ m for visible light.[50]

A schematic diagram of a typical SEM device is illustrated in Figure 26. The system consists of: an electron source; lenses and apertures; coils for rastering (scanning) the beam; control electronics and high-voltage supplies; a deflector/acquisition system for collecting and processing the signal information; a monitor to display the information; a vacuum system for the source, a column and a specimen chamber. [50]

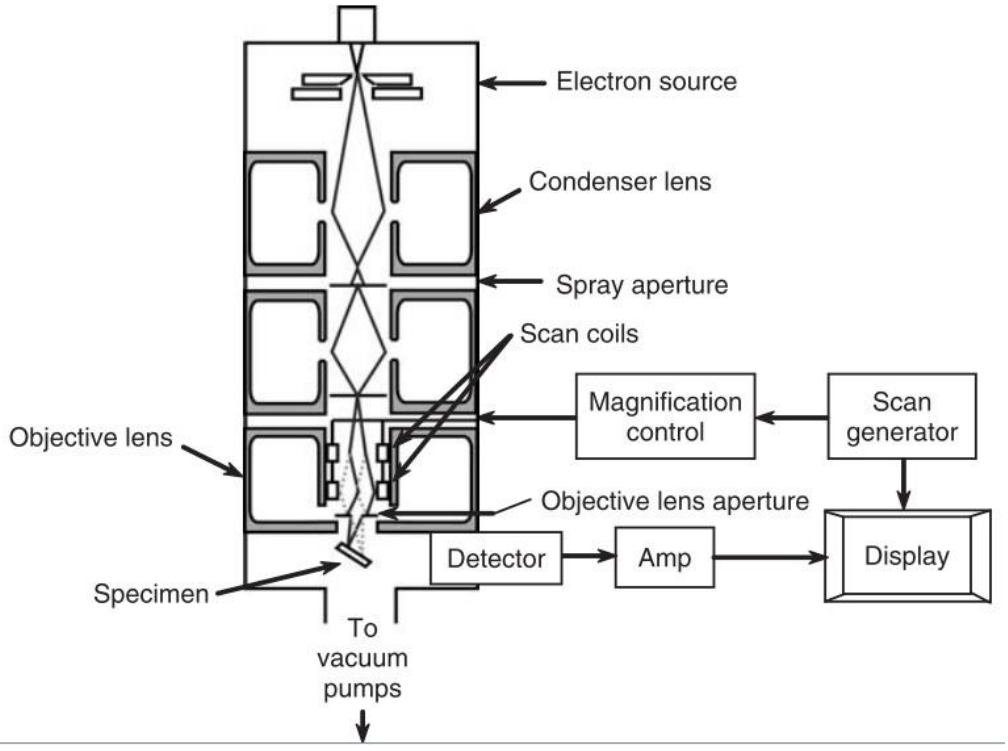


**Figure 26.** Simplified schematic diagram of the basic components of an SEM [51]

After the emission of electrons from the source (primary electrons), the beam is directed towards the sample using electromagnetic fields (condenser lenses). Interaction between the primary electrons and the material, as well as the generated signals are shown in Figure 27.

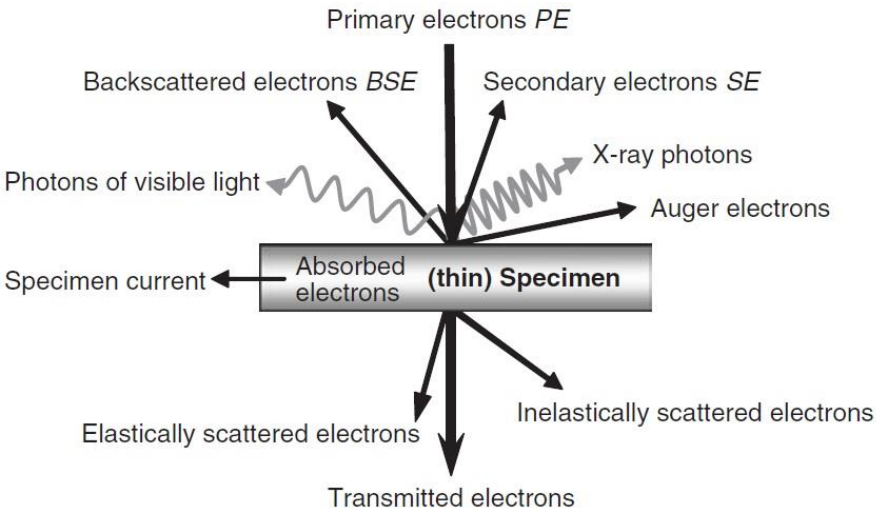


**Figure 27.** Signals that are generated when a focused electron beam strikes a specimen[50]

When a beam of primary electrons interacts with a material, there can be two typical outcomes. It could be inelastically scattered after the interaction with atomic electrons, emitting the electrons with the energy lower than about 50 eV called *secondary electrons (SE)*. The other possibility is to be elastically scattered by the atomic nucleus, creating the electrons with the energy greater than 50 eV, called *Backscattered electrons (BSEs).* Backscattering is more likely to occur for the elements with a higher atomic number. This is what is seen as a contrast in the final picture, given that the elements from high-Z region will produce higher brightness regions.[52]

What is making this method so widely used is that it is not restrictive in terms of sample requirements. Samples must be conductive and vacuum compatible, due to the high vacuum in the camber. For samples that are insulators, those must be coated with thin films of carbon, gold or some other conductive material.[52]

In this work, *Hitachi SU-70* scanning electron microscope was used with Accelerating Voltage of 20 kV. Used magnification was between 30 and 15000 times. Non-conductive samples were treated with gold, using a low-vacuum sputter deposition.

#### 11.3.2.1. EDS

As shown in Figure 27, one additional species that are generated after interaction with primary electrons are X-ray photons. These are formed as a side effect of electron transition from a higher excited state to the lower one.[50], [53] Detailed description of this process is given in Figure 28.

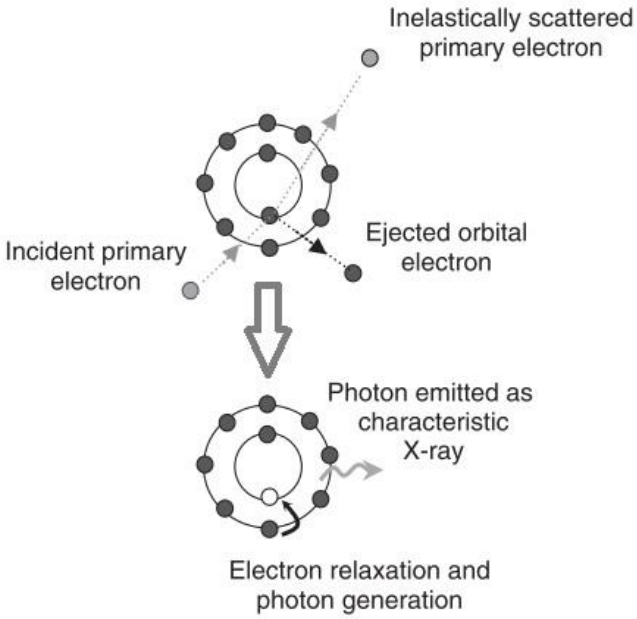


**Figure 28.** Schematic illustration of the process characteristic X-ray emission [50]

Signals created in this way could be analyzed in order to determine the chemical composition of materials, since every element will create its own distinct X-ray spectra. The most common analysis of this type is known as *Energy Dispersive X-ray spectroscopy (EDS).*[50]

### 11.3.3. Profilometry

*Veeco Dektak® 150 Surface Profiler* used in this work is a stylus type instrument widely used for measuring surface topography. The basic principle of this instrument is a conversion of the vertical movement of the stylus in contact with the sample surface into an electrical signal. Components of the typical surface profiler are shown in Figure 29.[54]

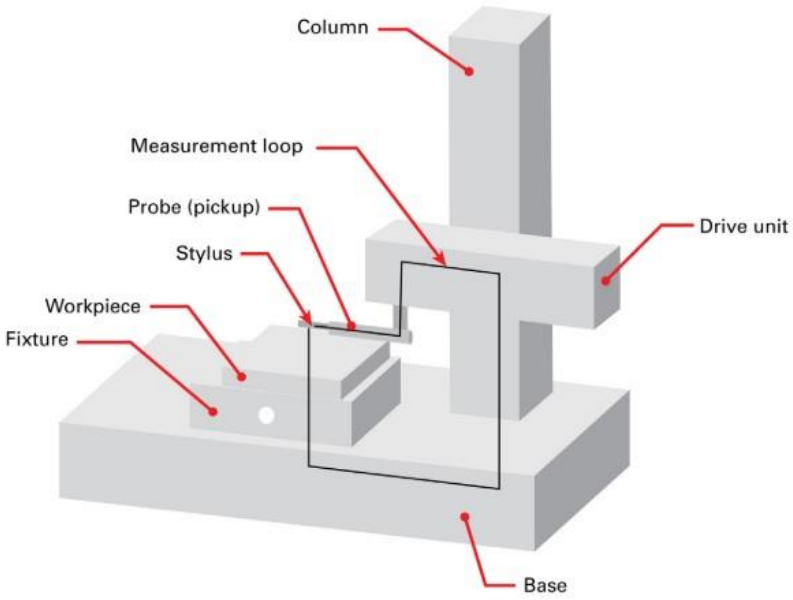


**Figure 29.** Schematic representation of a typical stylus instrument [54]

On this occasion, the surface profiler was used only to precisely measure the thickness of formed thin and thick films.

### 11.3.4. Four-Probe Resistivity

One of the most important parameters of conductive materials is its resistivity (or conductivity) since it can describe the material's performance in a circuit. There is a number of techniques to determine this property, but the one chosen in this work was four-probe resistivity measurement or the Kelvin method.

What makes this measurement convenient to use is that it is an absolute measurement without the need for standards. As the name suggests, it consists of four probes equally distant from one another. The contact arrangement of these with the measuring instrument (*Keithley 2400 SourceMeter SMU* in this case) is presented in Figure 30. [55]

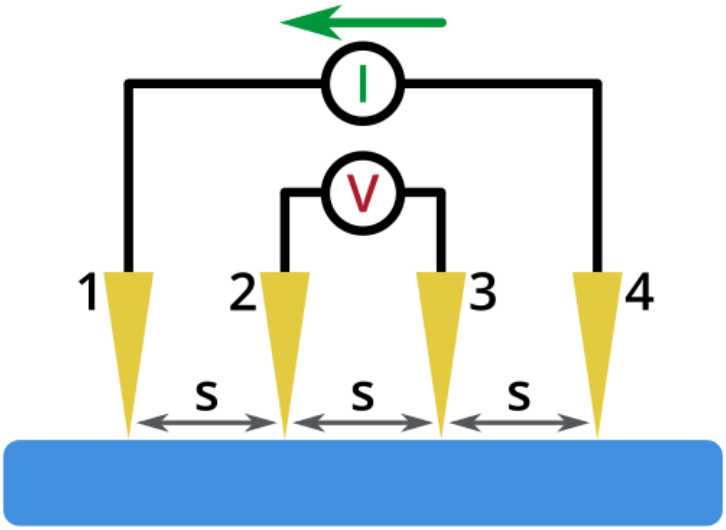


**Figure 30.** Four-terminal resistance measurement arrangements

The operational principle is that the voltage drop is measured between the two inner probes while a current ***I*** is applied the two outer probes. When the spacing between the probes ***s*** is uniform, the resistivity is

$$\rho = \left(\frac{\pi t}{\ln(2)}\right) \cdot \frac{V}{I} \text{ [Ω cm]} \qquad \text{for } s>>t,$$

where ***t*** represents film thickness. [55] From this, the sheet resistance is calculated using:

$$Rs = \frac{\rho}{t} = \left(\frac{\pi}{ln2}\right) \cdot \frac{V}{I} = 4.53 \cdot \frac{V}{I} \text{ [Ω]. [55]}$$

Finally, in order to get the true value, the geometrical correction factor must be applied. For a rectangular-shaped sample, a set of empirically determined values presented in Table 1 is used.

**Table 1.** Values of the correction factors for different probe spacings **s**, sample width ***w***, and sample length ***l*** vary

| w / s | l / w = 1 | l / w = 2 | l / w = 3 | l / w = 4 |
|---|---|---|---|---|
| 1 | | | 0.2204 | 0.2205 |
| 1.25 | | | 0.2751 | 0.2751 |
| 1.5 | | 0.3263 | 0.3286 | 0.3286 |
| 1.75 | | 0.3794 | 0.3803 | 0.3803 |
| 2 | | 0.4292 | 0.4297 | 0.4297 |
| 2.5 | | 0.5192 | 0.5194 | 0.5194 |
| 3 | 0.5422 | 0.5957 | 0.5958 | 0.5958 |

One sample during measurement is presented in Figure 31.

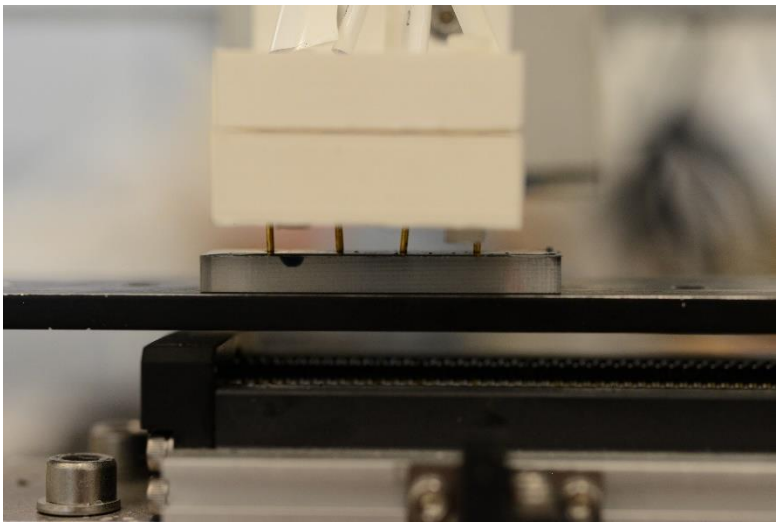

**Figure 31.** Four-probe resistivity measurement

All the dimensions needed to calculate the resistance are given in Table 2.

**Table 2.** Dimensions needed for four-probe resistivity

| Dimension | Value (mm) |
|---|---|
| Probe Spacing | 7 mm |
| Sample Width | 10 mm |
| Sample Length | 50 mm |

Based on these, the correction factor value of 0.4297 was chosen, making the final formula:

$$R_s = 1.95 \cdot \frac{V}{I} [\Omega]$$

### 11.3.5. Discharge Test

In accordance with the previously mentioned information, some of the most important battery parameters are *discharge time*, *capacity* and *energy density*. All of these could be obtained simply by performing the discharge test.

Discharge tests are carried out by applying a constant current on the battery while measuring the difference in potential that it generates over time. The discharge time of a battery varies according to the load to which it is subjected, so it is necessary to choose a suitable load. [2] In this particular work, it was 200 µA.

To ensure a good contact, the tool shown in Figure 32 was created. It was designed in *SolidWorks 2017* software and made with the *Ultimaker3* 3D printer.

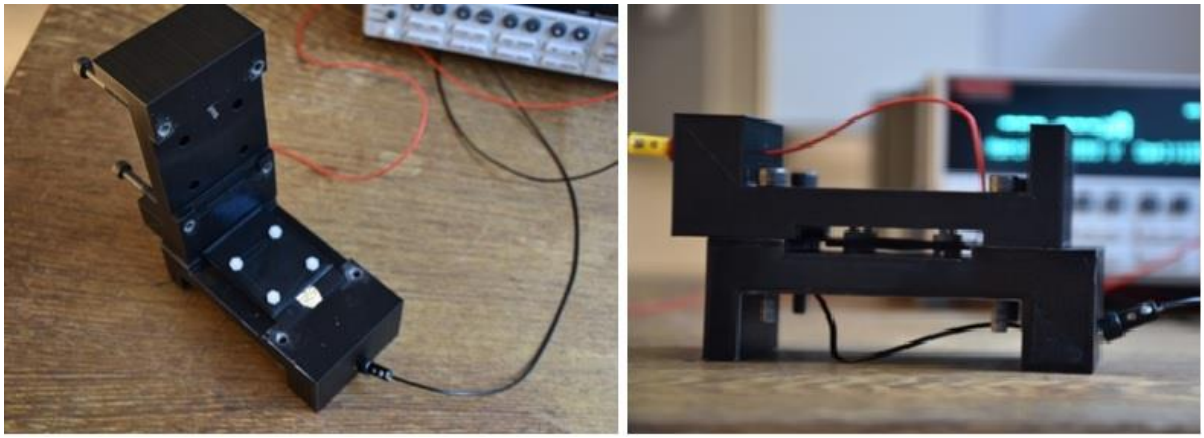

**Figure 32.** Battery holder for discharge test

The setup presented in Figure 33 was completed with *Keithley 2400 SourceMeter SMU* measuring instrument. All the data were recorded using *KickStart I-V Characterization* software.

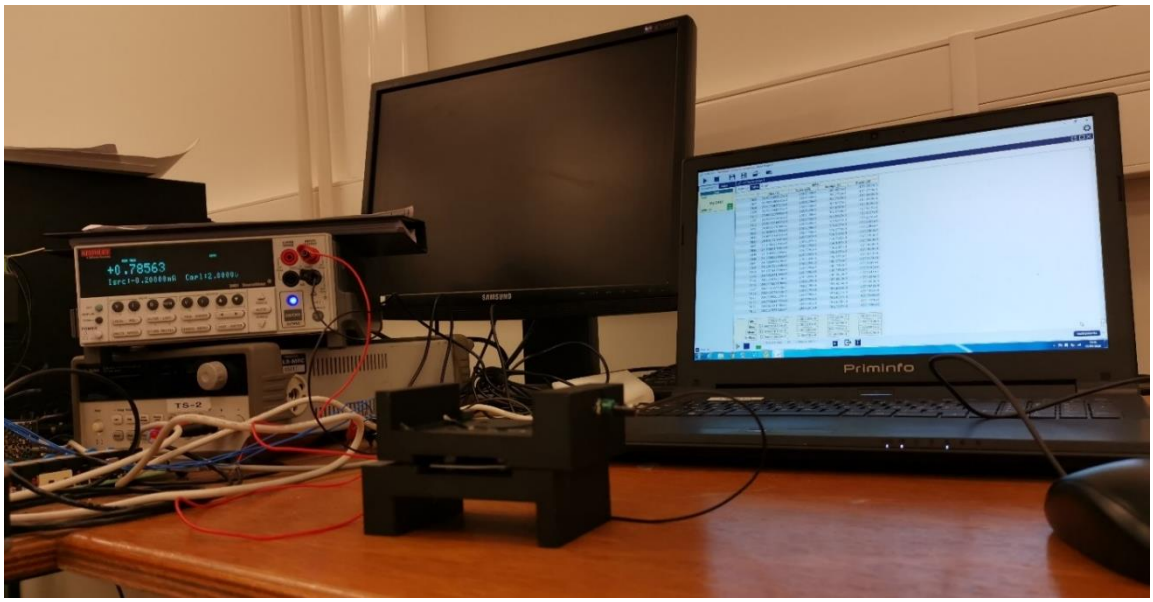


**Figure 33.** Discharge test setup

## 11.4. Sensing Properties

In order to test the sensing properties of this device, the same discharge test was performed. Difference was in the assembly design. A few changes were enforced. First, PLA support on the PEDOT:PSS side was done with a hole in the middle. Second, a hole was cut in PEDOT:PSS film, leaving the exposed separator (filter paper). Lastly, the filter paper was not impregnated with PBS.

After the assembly of the battery (Figure 34), it was connected to the Source Meter and the discharge test without the voltage bias was started and the current was measured. After the start, 0.5 mL of PBS was added directly on to the separator, triggering the response. This test was designed to mimic the real situation where this device would be sensing the bodily fluid, e.g. blood from a wound.

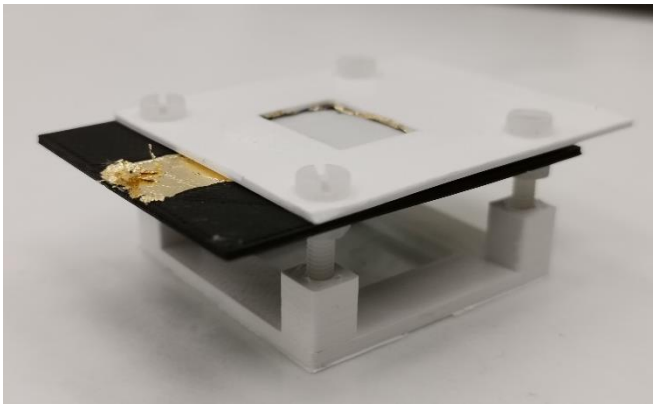

**Figure 34.** Device assembled for sensing test

# 12. Results and Discussion

## 12.1. Electrode

In order to produce samples with right dimensions and morphology, a number of different support and mold shapes were tried. On top of that, as already mentioned, different thermal treatments were tested. Even after this careful preparation, cracks could not be avoided in some samples, leading to a conclusion that those formulations are not suitable for this application (Figure 35).

**Figure 35.** Some different successful and less successful samples

The image of a successfully produced thin film and thick film electrode is shown in Figure 36.

**Figure 36.** Thin film electrode on a support (left) and thick film electrode in a mold (right)

Presumably the best difference in structure of the thick film with and without $CuCl_2$ can be seen in Figure 37.

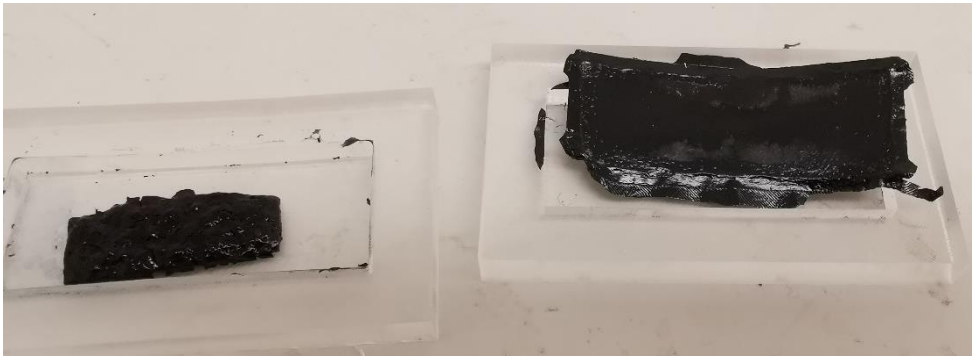

**Figure 37.** Difference between thick film with salt (left) and without salt (right)

Although this is not a very precise estimate, the difference in shape and size is evident. Even though these films were treated in the equal manner, the one with salt appears to have shrunk more. Moreover, it is visibly wet, entrapping water from the solution. Because of that, it is not suitable for use in batteries, but could be a good precursor for aerogels just as suggested by *Chen et. al.*[56]

### 12.1.1. Four-Probe Resistivity

In Table 3 are presented average resistance values of different films.

**Table 3.** Obtained values for film resistance

| | Film type | IL (w%) | $CuCl_2$ (mol%) | Rs (Ω) |
|---|---|---|---|---|
| 1 | Thin Film | 15% | - | 3.9975 |
| 2 | | 30% | | 1.51996 |
| 3 | | 45% | | 1.84661 |
| 4 | | 60% | | 1.63176 |
| 5 | Thin Film | 45% | 1% | 2.03844 |
| 6 | | | 3% | 2.56458 |
| 7 | | | 5% | 2.60386 |
| 8 | Thick Film | 0% | - | 21.8834 |
| 9 | | 15% | | 1.04689 |
| 10 | | 30% | | 0.71507 |
| 11 | | 45% | | 0.98976 |
| 12 | | 60% | | 0.54054 |
| 13 | Thick Film | 45% | 1% | 0.52195 |
| 14 | | | 3% | 0.72547 |
| 15 | | | 5% | 0.63109 |
| 16 | | | 10% | 0.33202 |

What is immediately clear is that the values for the pure PEDOT:PSS thin film and for the thin film with 10 mol% of copper(II)-chloride are missing. That is because it was impossible to obtain these

films, either because forming a film on a highly hydrophobic PDMS support was unachievable or the material is so brittle after thermal treatment that only small flakes are formed, rather than a uniform unbroken film.

Other noticeable value is that of the pure PEDOT:PSS film. It is the highest registered, but still rather low. Even though it could be considered satisfactory, this film is so brittle that it could not be used for this or any similar purpose. All other values are around 1 Ω, so taking into account that this method is not extremely precise, it is hard to differentiate them. That being said, resistance will not be the deciding factor for which the material will be further tested in batteries. That will be the mechanical characteristic of the films. Therefore, thick and thin films without $CuCl_2$ and with 60 w% of IL were chosen, since these were the most compact, easiest to spread and the most flexible and bendable ones.

### 12.1.2. Film Thickness

As previously mentioned, profilometry was done in order to precisely determine the film thickness. In Figure 38 is represented the typical profile for a thick film. It can be seen that the thickness on the edges is much higher. That is because of the making process and it is not influencing the result, since this part was cut when used in batteries. Thickness was determined based on the difference between the starting point (which is the glass support of the instrument) and the constant part of the graph.

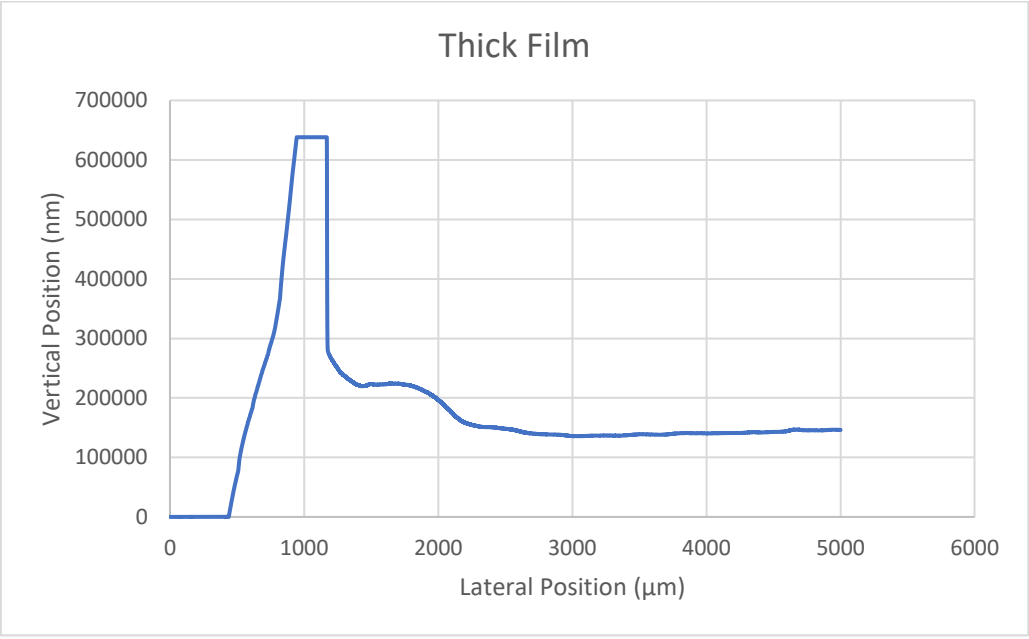


**Figure 38.** Thick film profile

Figure 39 shows that the profile of the thin film is similar to the thick film profile. Once again, thickness was determined based on the difference in vertical position of the support (zero point) and the smooth part of the film. It can immediately be seen that this film is significantly thinner.


**Figure 39.** Thin film profile

The results of thickness calculated by the used software were **21 µm** for the thin film and **142 µm** for the thick film.

### 12.1.3. SEM

In this chapter, SEM and EDS analyses of the made films are presented. In Figure 40, SEM images of the film with and without $CuCl_2$ can be seen at the magnification of 30 times. What is noticeable is that no significant forms or any zones of interest are present at this magnification. The same could be said for magnifications up to 2000 times. When analysis at higher magnifications was tried, the material started to melt due to the inability to withstand the excess heat of the powerful electron beams.

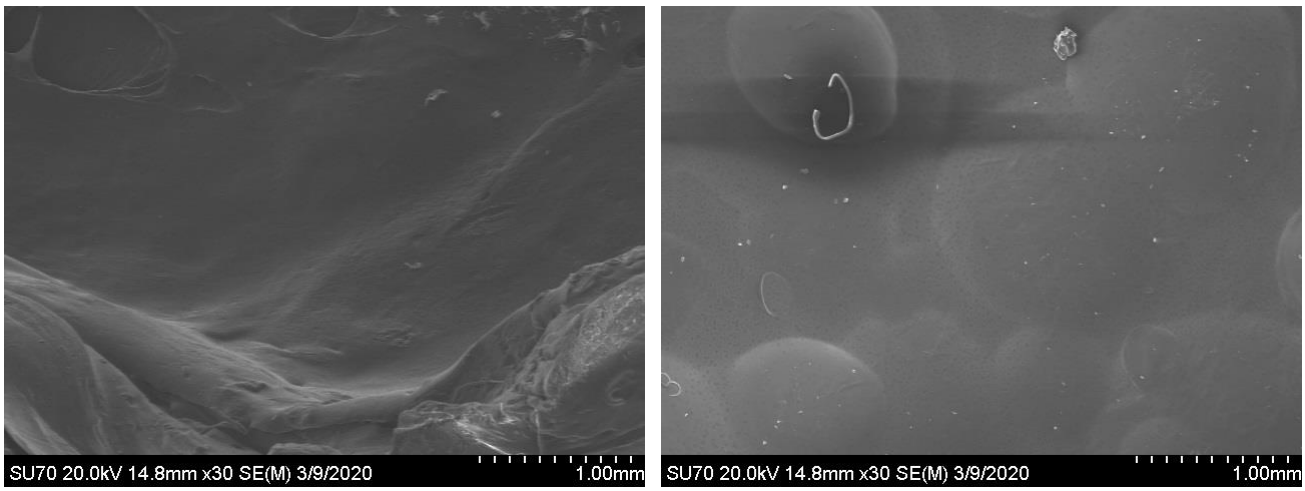


**Figure 40.** SEM images of the films with (left) and without (right) $CuCl_2$, x30

What was noticed during the process of film formation (after drying or after thermal treatment) is that occasionally crystal-like forms would appear in the samples (Figure 41).

The crystal formation was happening irrespective of the film form or film formulation, so it was concluded that it is not due to the copper(II) chloride or the formation process. EDS analysis was done on a number of different samples with the sole purpose of determining the composition of these crystals. All of these led to the same result and conclusion, one of which is presented in Figure 42.

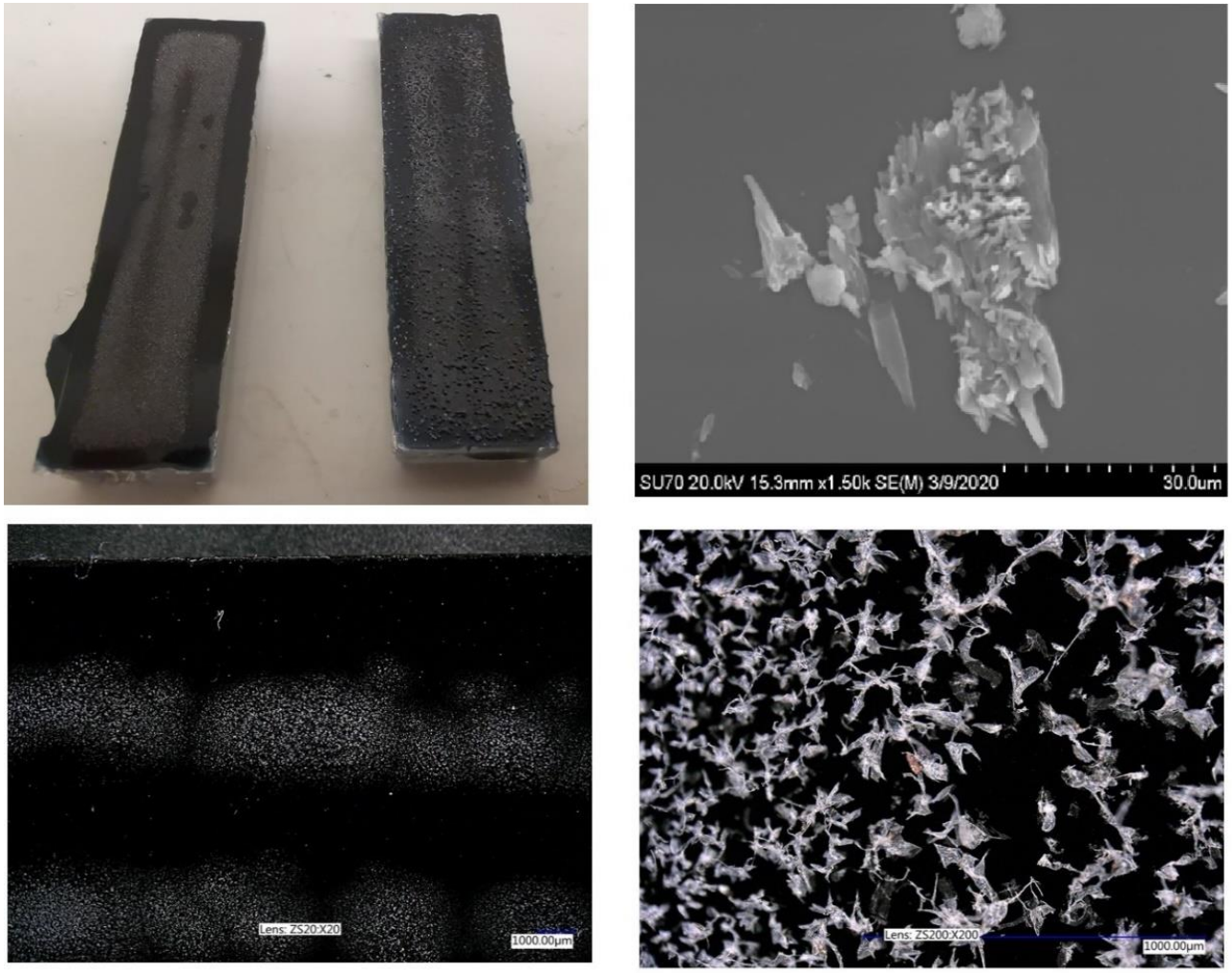


**Figure 41.** Different examples of formed crystals; a photo, SEM image x1500, microscope image x20, microscope image x200, respectively

Looking at the result for the *selected area 2* in Figure 42, only sulfur, oxygen and carbon are present, indicating that it is the PEDOT:PSS structure. On the other hand, EDS spectra for *selected area 1* shows peaks only for sulfur, oxygen, and sodium. This leads to a single conclusion that the crystals in question are **sodium-sulfate**. Given that sodium was not added in the mixture in any form, one can assume that it originated from the environment or some other unaccounted source.

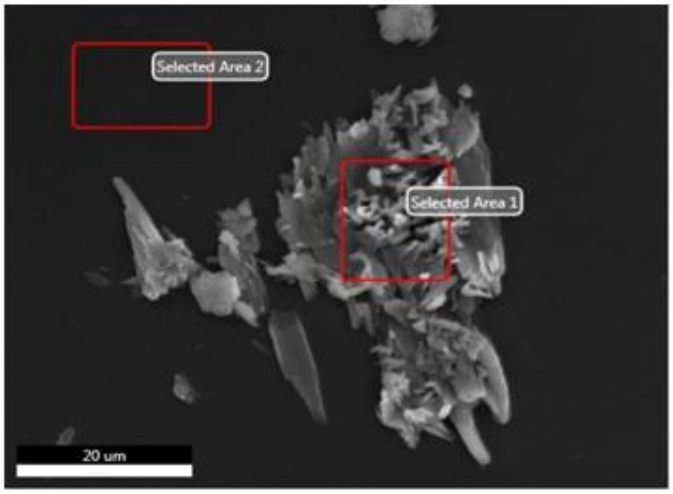


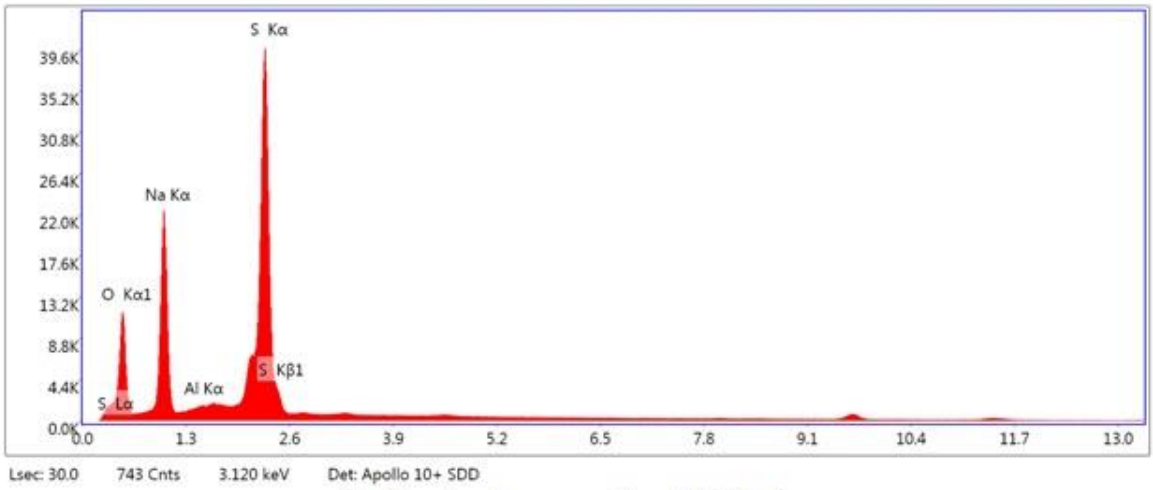


**Selected area 1 - EDS 1**

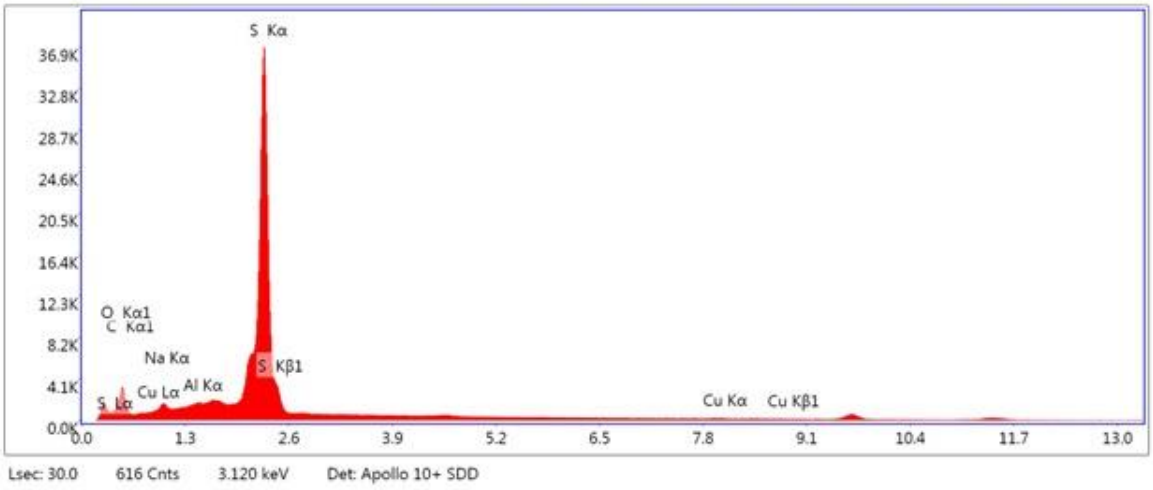


**Selected area 2 - EDS 2**

**Figure 42.** SEM and EDS analysis of the formed crystals

All samples like this were discarded and were not further used.

### 12.1.4. FTIR

In Figure 43, FTIR spectra of different PEDOT:PSS films are shown. This is done in order to determine whether some new chemical forms are created. What can be seen is that the spectra are very similar, and the only difference is in the intensity of the peaks. The similarity proves that there is no chemical reaction between the ionic liquid and PEDOT or PSS, just as it was suggested by *Wang et. al.* .[57]

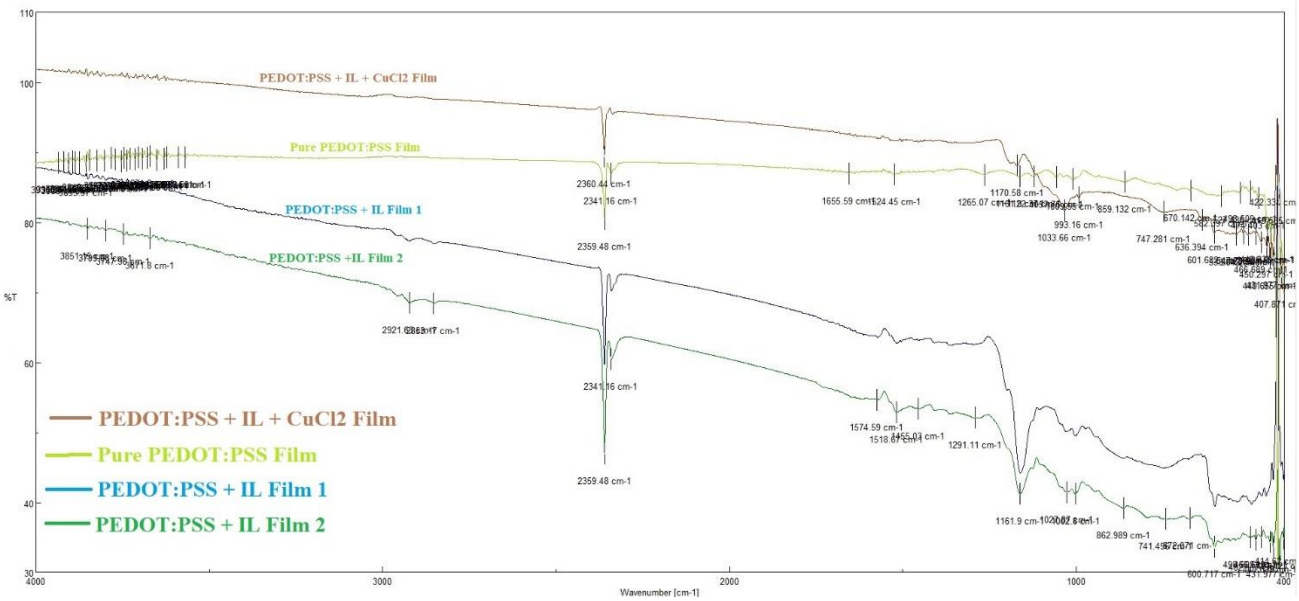


**Figure 43.** FTIR spectra of different PEDOT:PSS films

## 12.2. Battery

### 12.2.1. Discharge Test

In Figure 44, a typical thin-film battery discharge curve is shown. One can distinguish three regions:

1. The initial voltage drop as a result of polarization phenomena occurring during the assembly of the battery;
2. Region of the constant voltage for hours;
3. And lastly, another sudden voltage drop at around 0.2 V, marking the end of the discharge process.

Based on the result presented in Figure 44, thin-film battery discharge time, capacity, power, and energy were determined. Just by observing the curve, it is visible that the discharge time is around **18 h** at the discharge voltage of **0.2 V**. This gives:

$$C = I_d \cdot \tau_d = 0.2\,mA \cdot 18\,h = 3.6\,mAh$$

$$P = \varepsilon_d \cdot I_d = 0.2\,V \cdot 0.2\,mA = 0.04\,mW$$

$$E = P \cdot \tau_d = 0.04\,mW \cdot 18\,h = 0.72\,mWh$$

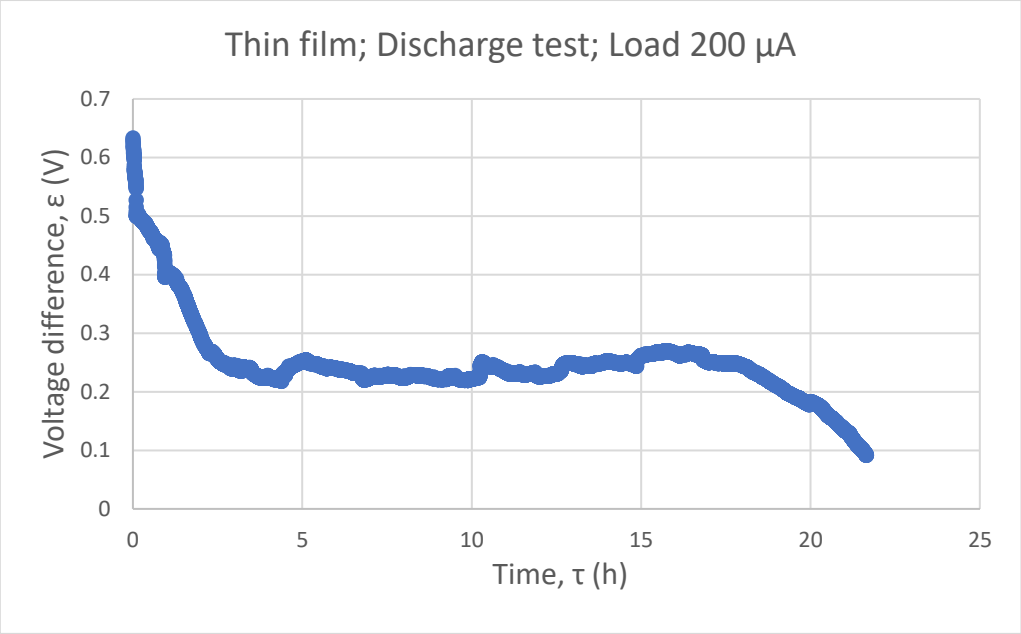


**Figure 44.** Thin-film battery discharge curve

Figure 45 presents a typical thick-film battery discharge curve. The trend of the curve is the same one as in the previous case, but this time the curve is stabilized at a much higher voltage, around 0.7 V. Unfortunately, this particular test had to be terminated due to the time constrains, so the final discharge time was impossible to determine, although the trend is clearly visible.

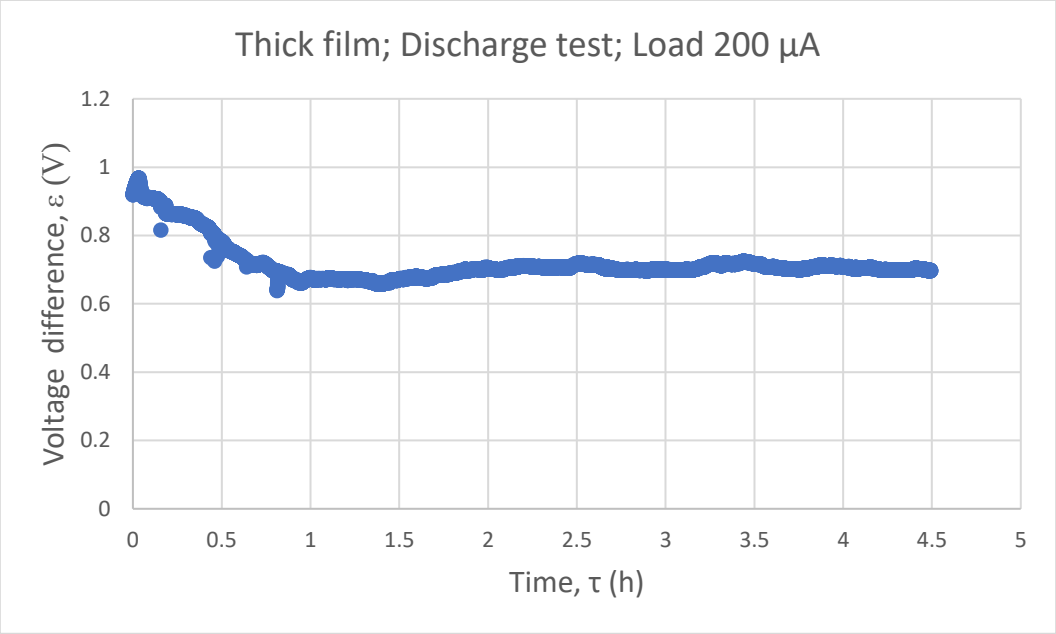


**Figure 45.** Typical thick-film battery discharge curve

The best obtained result for a thick-film battery is shown in Figure 46. Based on it, thick-film battery discharge time, capacity, power and energy were determined.

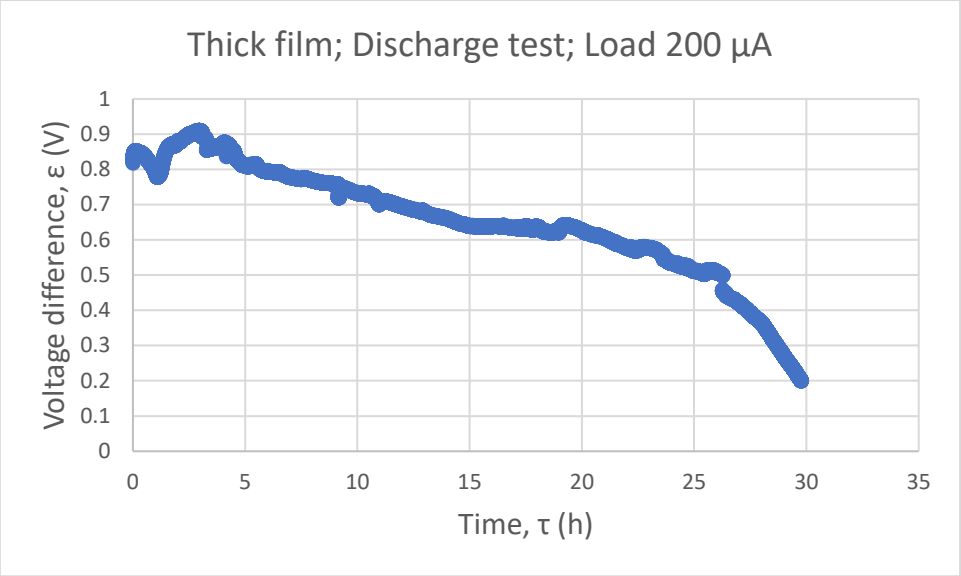


**Figure 46.** The best result for thick-film discharge curve achieved

Following the same procedure as for the thin film, it was established that the discharge time $\tau_d$ is **26 h** at the discharge voltage $\varepsilon_d$ of **0.5 V**

$$C = I_d \cdot \tau_d = 0.2\ mA \cdot 26\ h = 5.2\ mAh$$

$$P = \varepsilon_d \cdot I_d = 0.5\ V \cdot 0.2\ mA = 0.1\ mW$$

$$E = P \cdot \tau_d = 0.1\ mW \cdot 26\ h = 2.6\ mWh$$

## 12.3. Battery Reaction

After every discharge test was done, batteries were disassembled, visually inspected, and then further analyzed, as previously described. Figure 47 shows how battery components look before and after the discharge test.

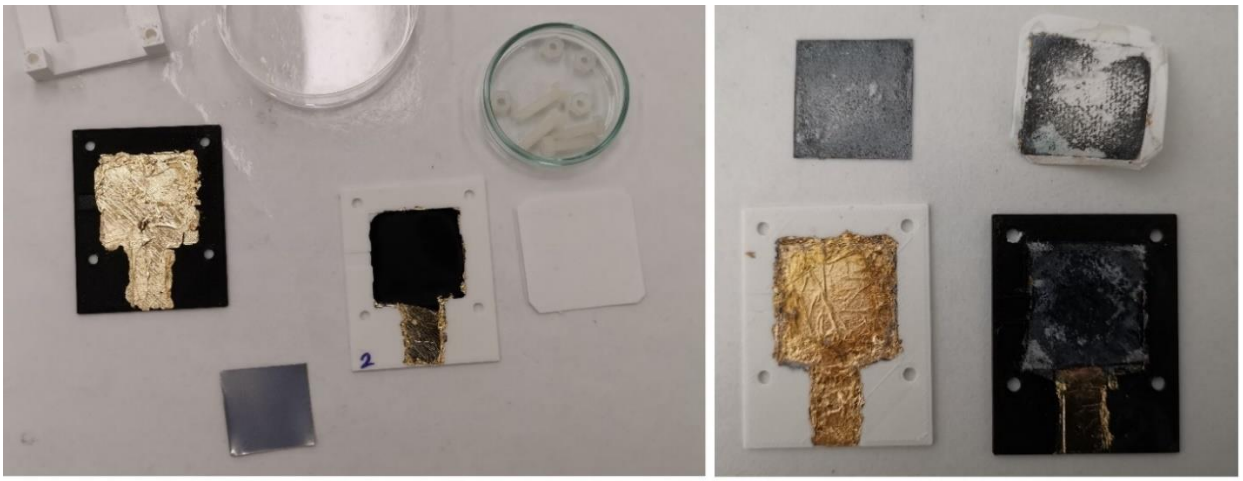

**Figure 47.** Battery components before (left) and after (right) discharge test

Just based on the visual inspection, it is clear that some kind of a process is occurring during the discharge.

### 12.3.1. SEM

Figure 48 represents the first step towards detailed analysis of the battery reaction.

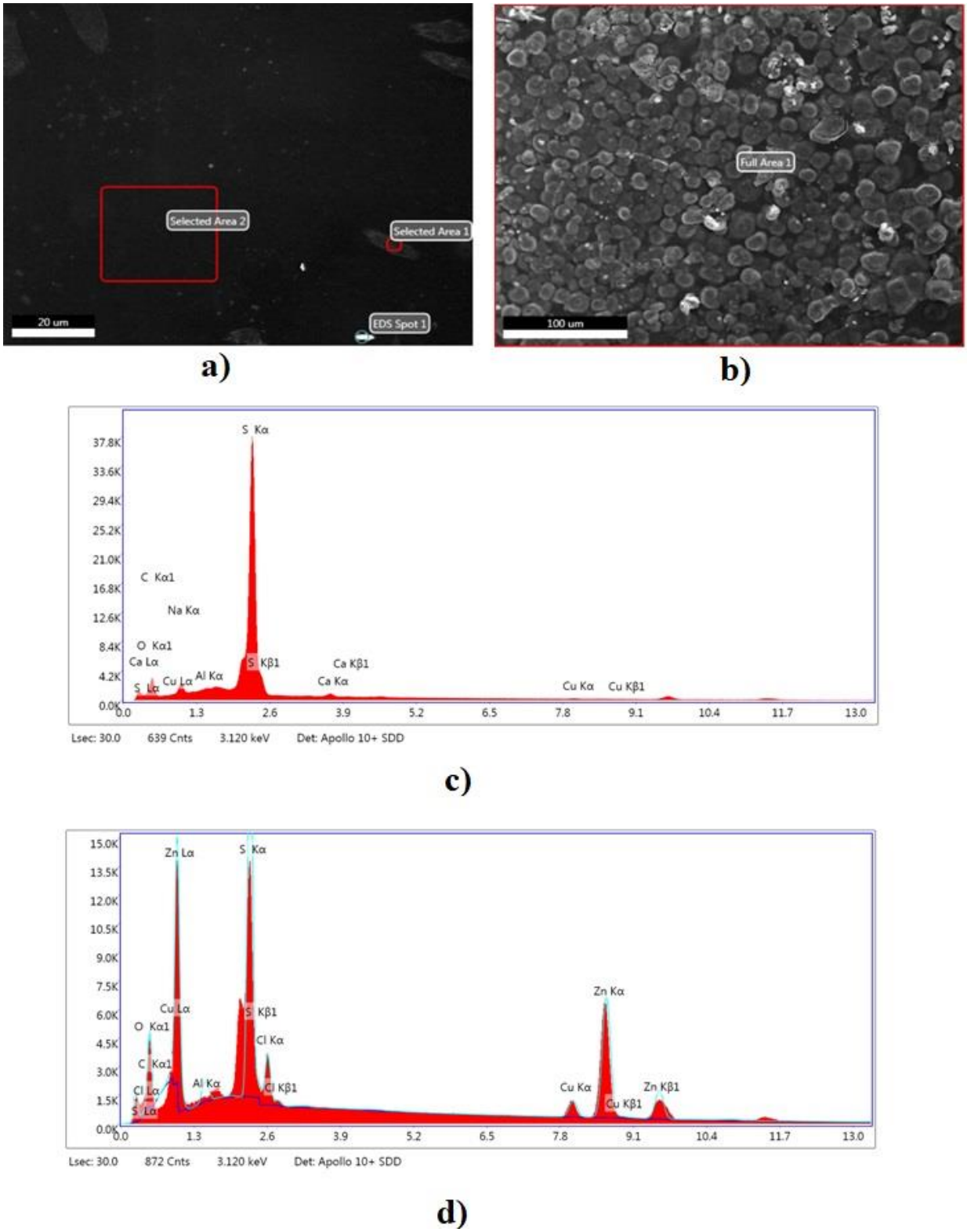


**Figure 48.** SEM images and EDS spectra for PEDOT:PSS electrode before (a and c) and after (b and d) discharge test

Images a and b are the result of SEM microanalysis at the magnification of 300 times. It is clearly seen that new forms appeared on the surface of the electrode. Comparing the EDS spectra shown in c and d on the same figure, one can see that the oxygen content is increased and that the peak belonging

to zinc appeared, leading to the conclusion that mentioned forms are zinc-oxide particles. This alone could be enough to conclude that the assumed reaction is occurring.

In addition to the electrode, the separator (filter paper) was analyzed after the discharge (Figure 49).

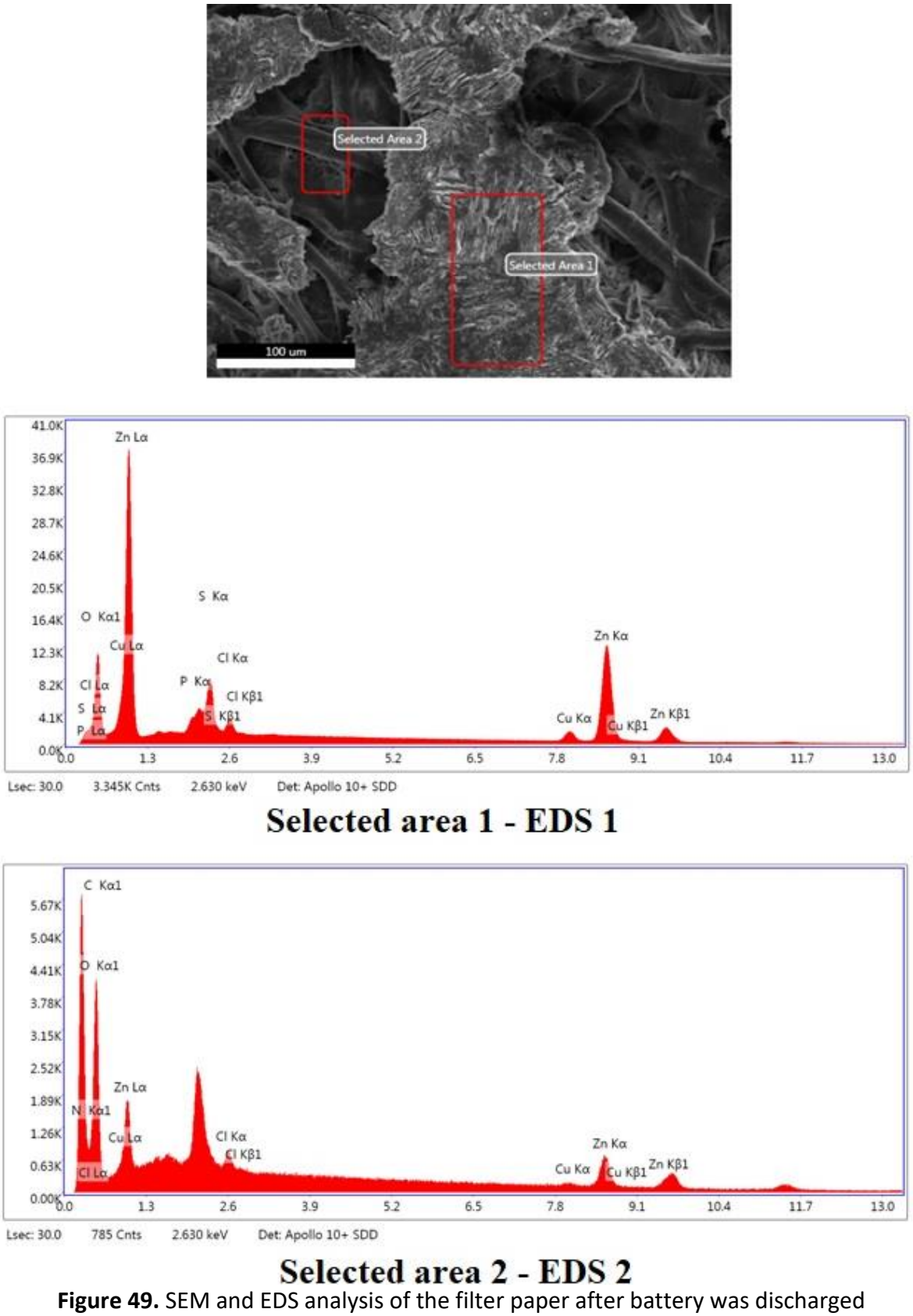


**Figure 49.** SEM and EDS analysis of the filter paper after battery was discharged

The fiber-like structure of the *Selected Area 2* suggests that this is a filter paper. This is also proven with its EDS, which predominantly shows carbon and oxygen, the components of cellulose. On the other hand, crystals formed in *Selected Area 1* must be ZnO since their EDS spectrum shows zinc and oxygen. This is further proof that the reaction is occurring and that the exchange of ions is present.

### 12.3.2. FTIR

In order to determine the composition of the material formed on the Zn-electrode, FTIR of this residue material was done. The resulting spectrum is shown in Figure 50.

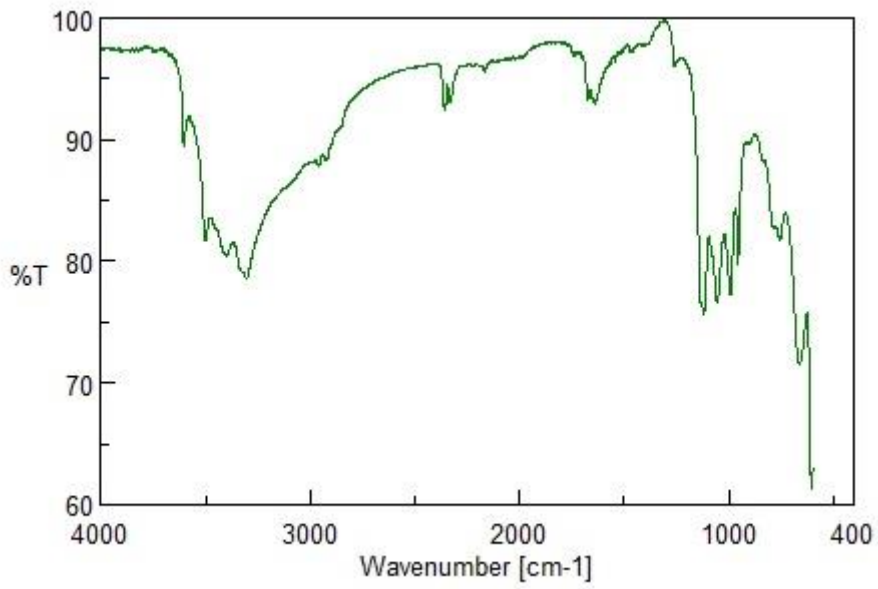


**Figure 50.** FTIR spectra of Zn-electrode residue

Although at the time of the analysis it was not possible to do a measurement under 600 $cm^{-1}$, it is clear that a sharp peak under 650 $cm^{-1}$ is present, the one characteristic of zinc-oxide[58][59]. This is a strong indication that ZnO is formed during the use of the battery.

The wide peak around 3300 $cm^{-1}$ can be attributed to O-H stretching, probably originating from adsorbed water.[58] All other peaks are suggesting an organic molecule (C=C stretching between 1600 and 1700 $cm^{-1}$, C-O stretching around 1200 $cm^{-1}$ and C-H bending around 1000 $cm^{-1}$).[60] Given that the analyzed material was in contact with filter paper, this organic molecule shown in the spectrum is cellulose.

## 12.4. Device Application

Results of the sensing test are presented in the Figure 51.

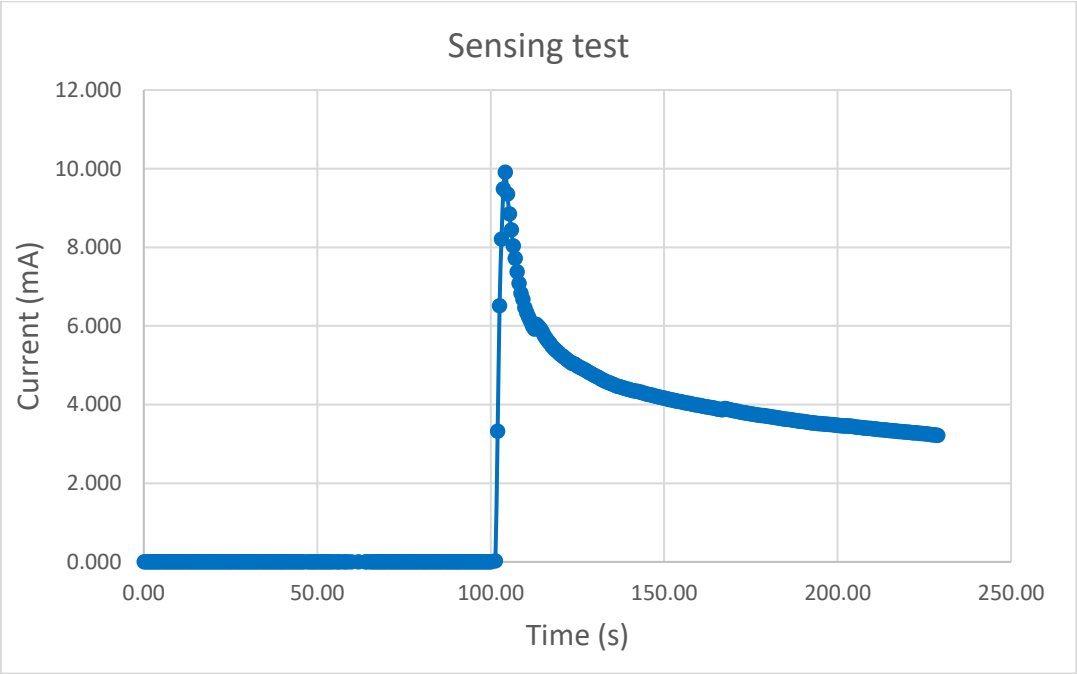


**Figure 51.** Sensing test

What can clearly be seen is that the response to the applied stimuli, which is in this case addition of 0.5 mL of PBS, is practically immediate. This is the proof that this device has a promising application as the sensor for biological application, as proposed. However, there is still an array of possibilities for research and improvement in terms of size, flexibility, and sheer performance.

# 13. Conclusions and Further Possibilities for Research

The primary aim of this research project was to explore the possibility of using a PEDOT:PSS films in energy storage systems and in sensing systems, as well as to further characterize the influence of film formation and formulation on its conductivity and overall performance in aforementioned systems. All of the findings are here briefly summarized.

As far as **electrode** is concerned,

- 1-butyl-3-methylimidazolium octyl sulfate ionic liquid proved to be crucial for film formation, as well as a significant conductivity enhancer, achieving the films with resistivities as low as 0.33 Ω;
- Although no significant change in resistivity was registered between films with and without copper(II)-chloride, the ones without it could be considered better performing, since their formation process was much easier and effortlessly repeatable;
- And FTIR analysis suggested that during the formation process of the films no significant change in chemical structure was present.

Concerning the **battery** as a system and its performance,

- It has a typical discharge curve for one galvanic cell with an initial voltage drop, followed by a region of constant voltage finished by a sudden voltage drop;
- In terms of film thickness, thick films proved to have both higher discharge voltage and longer discharge time, resulting in the higher capacity and power, proving to be a better solution for this system.
- The best battery had a power of 0.1 mW, which could be used for the Endoscopy capsule, as shown in Figure 2.

The analysis of the **electrochemical reaction** occurring in the battery during discharge led to the following conclusions:

- SEM and EDS analysis of the formed structures on the Zn-electrode and on the separator showed that those are zinc-oxide crystals, proving that the oxidation on zinc is occurring and that the reaction is consistent with that of a Zn-air battery;
- Further proof in favor of the same reaction gave the FTIR analysis of the surface of the Zn-electrode, which showed peaks consistent with the ZnO.

In the final stage of the research it was proved that with minimal adaptation, the same system could be used as a **sensor** for electrolytes (in this case it was PBS), which leads to a reasonable conclusion

that the same system could be used for detecting liquids, such as bodily fluids. This opens the possibility of adapting it to be able to detect and monitor wounds on the human body.

In terms of the future work and possibilities, many different aspects could be explored:

- Mechanical testing of both the electrodes and the whole system should be done in order to definitively prove its flexibility;
- In terms of the battery application:
    - Specific surface of the anode should be increased in order to achieve better performance,
    - Shape, size and the packing of the battery as a product represents a challenge which could lead to the exciting results,
    - Using these batteries in a series for powering devices with greater power should be tested as well.
- As far as exploring the sensing abilities of this system is concerned, more work should be devoted to:
    - Detailed analysis of the properties and the monitoring abilities;
    - Better packaging, specifically shape, size and wearing ability;
    - Overall performance of the device.

# 14. References


[1] X. Jia *et al.*, "Biocompatible ionic liquid-biopolymer electrolyte-enabled thin and compact magnesium-Air batteries," *ACS Appl. Mater. Interfaces*, vol. 6, no. 23, pp. 21110–21117, 2014.

[2] P. Westbroek, *Fundamentals of electrochemistry*. 2005.

[3] M. A. and J.-M. Tarascon, "Building better batteries," *Nature*, vol. 451, no. 7, pp. 652–657, 2008.

[4] K. Schmidt-Rohr, "How Batteries Store and Release Energy: Explaining Basic Electrochemistry," *J. Chem. Educ.*, vol. 95, no. 10, pp. 1801–1810, 2018.

[5] T. R. Crompton, *Battery Reference Book*, 3rd Editio. © Newnes 2000, 2000.

[6] F. Cheng and J. Chen, "Metal-air batteries: From oxygen reduction electrochemistry to cathode catalysts," *Chem. Soc. Rev.*, vol. 41, no. 6, pp. 2172–2192, 2012.

[7] J. S. Lee *et al.*, "Metal-air batteries with high energy density: Li-air versus Zn-air," *Adv. Energy Mater.*, vol. 1, no. 1, pp. 34–50, 2011.

[8] H. Arai, "Metal Storage/Metal Air (Zn, Fe, Al, Mg)," in *Electrochemical Energy Storage for Renewable Sources and Grid Balancing*, vol. 4, Elsevier B.V., 2015, pp. 337–344.

[9] Y. Li and J. Lu, "Metal-Air Batteries : Future Electrochemical Energy Storage of Choice?," *ACS Energy Lett*, vol. 2, no. 6, pp. 1370–1377, 2017.

[10] C. Wang *et al.*, "Recent progress of metal-air batteries-A mini review," *Appl. Sci.*, vol. 9, no. 14, pp. 1–22, 2019.

[11] R. Van Noorden, "The rechargeable revolution: A better battery," *Nature*, vol. 507, no. 7490, pp. 26–28, 2014.

[12] C. J. Lan, T. S. Chin, P. H. Lin, and T. P. Perng, "Zn-Al alloy as a new anode-metal of a zinc-air battery," *J. New Mater. Electrochem. Syst.*, vol. 9, no. 1, pp. 27–32, 2006.

[13] R. Cao, J. S. Lee, M. Liu, and J. Cho, "Recent progress in non-precious catalysts for metal-air batteries," *Adv. Energy Mater.*, vol. 2, no. 7, pp. 816–829, 2012.

[14] Y. Zhang *et al.*, "Confining iron carbide nanocrystals inside CNx@CNT toward an efficient electrocatalyst for oxygen reduction reaction," *ACS Appl. Mater. Interfaces*, vol. 7, no. 21, pp. 11508–11515, 2015.

[15] X. Lang, F. Ge, K. Cai, L. Li, Q. Wang, and Q. Zhang, "A novel Mn3O4/MnO nano spherical transition metal compound prepared by vacuum direct current arc method as bi-functional catalyst for lithium-oxygen battery with excellent electrochemical performances," *J. Alloys Compd.*, vol. 770, pp. 451–457, 2019.

[16] L. Qian *et al.*, "Trinary Layered Double Hydroxides as High-Performance Bifunctional Materials for Oxygen Electrocatalysis," *Adv. Energy Mater.*, vol. 5, no. 13, pp. 1–6, 2015.

[17] T. Maiyalagan, K. A. Jarvis, S. Therese, P. J. Ferreira, and A. Manthiram, "Spinel-type lithium cobalt oxide as a bifunctional electrocatalyst for the oxygen evolution and oxygen reduction reactions," *Nat. Commun.*, vol. 5, no. May, pp. 1–8, 2014.

[18] Y. Liu *et al.*, "Facile synthesis of spinel CuCo2O4 nanocrystals as high-performance cathode catalysts for rechargeable Li-air batteries," *Chem. Commun.*, vol. 50, no. 93, pp. 14635–14638, 2014.

[19] A. Indra *et al.*, "Unification of catalytic water oxidation and oxygen reduction reactions: Amorphous beat crystalline cobalt iron oxides," *J. Am. Chem. Soc.*, vol. 136, no. 50, pp. 17530–17536, 2014.

[20] N. Zhou, N. Wang, Z. Wu, and L. Li, “Probing active sites on metal-free, nitrogen-doped carbons for oxygen electroreduction: A review,” *Catalysts*, vol. 8, no. 11, 2018.

[21] X. Han, X. Wu, C. Zhong, Y. Deng, N. Zhao, and W. Hu, “NiCo2S4 nanocrystals anchored on nitrogen-doped carbon nanotubes as a highly efficient bifunctional electrocatalyst for rechargeable zinc-air batteries,” *Nano Energy*, vol. 31, no. December 2016, pp. 541–550, 2017.

[22] P. Gu, M. Zheng, Q. Zhao, X. Xiao, H. Xue, and H. Pang, “Rechargeable zinc-air batteries: A promising way to green energy,” *J. Mater. Chem. A*, vol. 5, no. 17, pp. 7651–7666, 2017.

[23] I. Smoljko, S. Gudić, N. Kuzmanić, and M. Kliškić, “Electrochemical properties of aluminium anodes for Al/air batteries with aqueous sodium chloride electrolyte,” *J. Appl. Electrochem.*, vol. 42, no. 11, pp. 969–977, 2012.

[24] T. Kuboki, T. Okuyama, T. Ohsaki, and N. Takami, “Lithium-air batteries using hydrophobic room temperature ionic liquid electrolyte,” *J. Power Sources*, vol. 146, no. 1–2, pp. 766–769, 2005.

[25] X. Yu and A. Manthiram, “A Voltage-Enhanced, Low-Cost Aqueous Iron-Air Battery Enabled with a Mediator-Ion Solid Electrolyte,” *ACS Energy Lett.*, vol. 2, no. 5, pp. 1050–1055, 2017.

[26] J. Fu, Z. P. Cano, M. G. Park, A. Yu, M. Fowler, and Z. Chen, “Electrically Rechargeable Zinc–Air Batteries: Progress, Challenges, and Perspectives,” *Adv. Mater.*, vol. 29, no. 7, 2017.

[27] Y. Li and H. Dai, “Recent advances in Zinc-air batteries,” *Chem. Soc. Rev.*, vol. 43, no. 15, pp. 5257–5275, 2014.

[28] W. Tahil, “The Zinc Air Battery and the Zinc Economy : A Virtuous Circle,” *Meridian International Research*, pp. 1–9, 2007.

[29] “Scholar Plotr.” [Online]. Available: https://csullender.com/scholar/.

[30] P. Sapkota and H. Kim, “Zinc-air fuel cell, a potential candidate for alternative energy,” *J. Ind. Eng. Chem.*, vol. 15, no. 4, pp. 445–450, 2009.

[31] H. Shirakawa, E. J. Louis, A. G. MacDiarmid, C. K. Chiang, and A. J. Heeger, “Synthesis of electrically conducting organic polymers: Halogen derivatives of polyacetylene, (CH)x,” *J. Chem. Soc. Chem. Commun.*, no. 16, pp. 578–580, 1977.

[32] D. Fichou and G. Horowitz, “Molecular and Polymer Semiconductors, Conductors, and Superconductors: Overview,” *Encycl. Mater. Sci. Technol.*, pp. 5748–5757, 2001.

[33] C. K. Chiang *et al.*, “Electrical conductivity in doped polyacetylene,” *Phys. Rev. Lett.*, vol. 39, no. 17, pp. 1098–1101, 1977.

[34] P. Chandrasekhar, *Conducting Polymers, Fundamentals and Applications*, 1st editio. Springer, 1999.

[35] H. Heeger, Alan J. ; MacDiarmid, Alan G. ; Shirakawa, “Advanced Information - The Nobel Prize in Chemistry 2000,” 2000.

[36] MCC Organic Chemistry, “Stability of Conjugated Dienes MO Theory.” [Online]. Available: https://courses.lumenlearning.com/suny-mcc-organicchemistry/chapter/stability-of-conjugated-dienes-mo-theory/.

[37] J. Tarver, J. E. Yoo, and Y.-L. Loo, “Organic Electronic Devices with Water-Dispersible Conducting Polymers,” in *Comprehensive Nanoscience and Technology*, 2011, pp. 413–446.

[38] F. Wolfart *et al.*, “Conducting polymers revisited: applications in energy, electrochromism and molecular recognition,” *J. Solid State Electrochem.*, vol. 21, no. 9, pp. 2489–2515, 2017.

[39] Y. Wen and J. Xu, “Scientific Importance of Water-Processable PEDOT–PSS and Preparation, Challenge and New Application in Sensors of Its Film Electrode: A Review,” *J. Polym. Sci. Part A Polym. Chem.*, vol. 55, no. 7, pp. 1121–1150, 2017.

[40] S. Kirchmeyer and K. Reuter, “Scientific importance, properties and growing applications of poly(3,4-ethylenedioxythiophene),” *J. Mater. Chem.*, vol. 15, no. 21, pp. 2077–2088, 2005.

[41] L. Groenendaal, F. Jonas, D. Freitag, H. Pielartzik, and J. R. Reynolds, “Poly(3,4-ethylenedioxythiophene) and its derivatives: past, present, and future,” *Adv. Mater.*, vol. 12, no. 7, pp. 481–494, 2000.

[42] W. Lövenich, “PEDOT-properties and applications,” *Polym. Sci. - Ser. C*, vol. 56, no. 1, pp. 135–143, 2014.

[43] H. Shi, C. Liu, Q. Jiang, and J. Xu, “Effective Approaches to Improve the Electrical Conductivity of PEDOT:PSS: A Review,” *Adv. Electron. Mater.*, vol. 1, no. 4, pp. 1–16, 2015.

[44] J. M. Gomes, S. S. Silva, and R. L. Reis, “Biocompatible ionic liquids: fundamental behaviours and applications,” *Chem. Soc. Rev.*, vol. 48, no. 15, pp. 4317–4335, 2019.

[45] M. Döbbelin *et al.*, “Influence of ionic liquids on the electrical conductivity and morphology of PEDOT:PSS films,” *Chem. Mater.*, vol. 19, no. 9, pp. 2147–2149, 2007.

[46] Y. Wang *et al.*, “A highly stretchable, transparent, and conductive polymer,” *Sci. Adv.*, vol. 3, no. 3, 2017.

[47] S. Li, “Monitoring Corrosion Using Vibrational Spectroscopic Techniques,” in *Intelligent Coatings for Corrosion Control*, Elsevier Inc., 2015, pp. 673–701.

[48] J. NEAL COX, “FTlR,” in *Encyclopedia of Materials Characterization*, no. 30, 1992, pp. 416–427.

[49] U. Junejo, “Working principle of ATR spectrometer,” 2017. [Online]. Available: https://upload.wikimedia.org/wikipedia/commons/2/28/Schematic_of_ATR-FTIR_Spectrometer.png.

[50] D. J. Stokes, *Principles and Practice of Variable Pressure/Environmental Scanning Electron Microscopy (VP-ESEM)*. 2008.

[51] J. I. Goldstein, D. E. Newbury, J. R. Michael, N. W. M. Ritchie, J. H. J. Scott, and D. C. Joy, *Microscopy and X-Ray Microanalysis*. 2018.

[52] J. B. Bindell, “2.2 Sem,” in *Encyclopedia of Materials Characterization*, 1992, pp. 70–84.

[53] R. H. Geiss, “EDS: Energy-Dispersive X-Ray Spectroscopy,” in *Encyclopedia of Materials Characterization*, 1992, pp. 120–134.

[54] R. Leach, *Surface topography measurement instrumentation*, Second Edi. Elsevier Inc., 2014.

[55] D. K. SCHRODER, *Semiconductor Material and Device Characterization*, 3rd Editio. A JOHN WILEY & SONS, INC., 2006.

[56] G. Chen *et al.*, “Strain- and Strain-Rate-Invariant Conductance in a Stretchable and Compressible 3D Conducting Polymer Foam,” *Matter*, vol. 1, no. 1, pp. 205–218, 2019.

[57] Y. Wang *et al.*, “A highly stretchable, transparent, and conductive polymer,” *Sci. Adv.*, vol. 3, no. 3, pp. 1–11, 2017.

[58] K. Sowri Babu, A. Ramachandra Reddy, C. Sujatha, K. Venugopal Reddy, and A. N. Mallika, “Synthesis and optical characterization of porous ZnO,” *J. Adv. Ceram.*, vol. 2, no. 3, pp. 260–265, 2013.

[59] COBLENTZ SOCIETY, “Zinc oxide IR Spectrum,” 2018. [Online]. Available: https://webbook.nist.gov/cgi/cbook.cgi?ID=B6004648&Mask=80.

[60] Sigma Aldrich, “IR Spectrum Table & Chart.” [Online]. Available: https://www.sigmaaldrich.com/technical-documents/articles/biology/ir-spectrum-table.html.

# 15. Bibliography


1. Hollas, J. M. (1996). Modern Spectroscopy (3rd ed.). John Wiley.
2. Brabazon, D. and Raffer, A. (2010) *Advanced Characterization Techniques for Nanostructures*. First Edit, *Emerging Nanotechnologies for Manufacturing*. First Edit. Elsevier Inc. doi: 10.1016/B978-0-8155-1583-8.00003-X.
3. Leach, R. (2014) Surface topography characterisation. Second Edition, Fundamental Principles of Engineering Nanometrology. Second Edition. Elsevier Inc. doi: 10.1016/B978-1-4557-7753-2.00008-6.
4. Park, J. B., Jeon, Y. and Ko, Y. (2015) 'Effects of titanium brush on machined and sand-blasted/acid-etched titanium disc using confocal microscopy and contact profilometry', *Clinical Oral Implants Research*, 26(2), pp. 130–136. doi: 10.1111/clr.12302.
5. Takahashi, S., Watanabe, K. and Takamasu, K. (2010) 'A novel resist surface profilometer for next-generation photolithography using mechano-optical arrayed probe system', *CIRP Annals - Manufacturing Technology*. CIRP, 59(1), pp. 521–524. doi: 10.1016/j.cirp.2010.03.145.
6. Vickerman, J. C. and Gilmore, I. S. (2009) Surface Analysis - The Principal Techniques: Second Edition, doi: 10.1002/9780470721582.
7. Redondo-Iglesias, E., Venet, P. and Pelissier, S. (2016) 'Measuring Reversible and Irreversible Capacity Losses on Lithium-Ion Batteries', *2016 IEEE Vehicle Power and Propulsion Conference, VPPC 2016 - Proceedings*. doi: 10.1109/VPPC.2016.7791723.
8. Abderrahim, B. *et al.* (2015) 'Kinetic Thermal Degradation of Cellulose, Polybutylene Succinate and a Green Composite: Comparative Study', *World Journal of Environmental Engineering, Vol. 3, 2015, Pages 95-110*, 3(4), pp. 95–110. doi: 10.12691/WJEE-3-4-1.
9. M. A. and J.-M. Tarascon, "Building better batteries," *Nature*, vol. 451, no. 7, pp. 652–657, 2008.
10. J. Koryta, J. Dvorak, and L. Kavan, *Principles of Electrochemistry*, 2nd editio., vol. 33, no. 1. John Wiley & Sons, Ltd., 1994.
11. K. Mullen and G. Wegner, *Electronic Materials: The Oligomer Approach*. WILEY-VCH, 1998.